

## Article

# Management of Natural Gas Consumption during the Manufacturing of Lead-Acid Batteries

Alexis Sagastume Gutiérrez <sup>1,\*</sup>, Juan Jose Cabello Eras <sup>2</sup>, Jorge Mario Mendoza Fandiño <sup>2</sup>  
and Humberto Carlos Tavera Quiroz <sup>2</sup>

<sup>1</sup> Energy Department, Universidad de la Costa, Calle 50 No. 55-66, PBX 336 22 00, Barranquilla 080002, Colombia

<sup>2</sup> Departamento de Ingeniería Mecánica, Universidad de Córdoba, Carrera 6 No. 77-305, Montería 230002, Colombia; juancabelloe@correo.unicordoba.edu.co (J.J.C.E.); jorge.mendoza@correo.unicordoba.edu.co (J.M.M.F.); humbertotaveraq@correo.unicordoba.edu.co (H.C.T.Q.)

\* Correspondence: asagastu1@cuc.edu.co

**Abstract:** The production of lead-acid batteries is an energy-intensive process where 28 to 35% of the energy is used in the form of heat, usually obtained from the combustion of fossil fuels. Regardless of the importance of heat consumption during battery manufacturing, there is no discussion available in the specialized literature that assesses heat during battery manufacturing. This study assessed natural gas consumption in a battery plant based on historical data, the thermographic evaluation of different equipment, and measurements of the combustion processes and combustion gases. Heat transfer models were used to calculate surface heat losses in the various assessed processes, while combustion theory was used to identify other saving potentials. Saving potentials equivalent to 16.6% of the plant's total natural gas consumption were identified. Replacing the ingot casting system accounts for a potential saving equivalent to 13.6% of the plant gas consumption, improving the grid casting systems for 2.8%, and the leady oxide accounts for a low 0.1%. Implementing the saving measures related to surface heat loss and poor operational practice reduced natural gas consumption by an estimated 1.2% monthly. Savings could be increased to 3.2% by expanding the saving measures to the remaining grid casting systems. Overall, natural gas consumption was reduced by an estimated 777 m<sup>3</sup>/month, GHG emissions by 1.6 tCO<sub>2eq</sub>/month, and fuel costs by 1603 USD/month.

**Keywords:** lead-acid battery; energy efficiency; thermal efficiency



check for updates

**Citation:** Sagastume Gutiérrez, A.; Cabello Eras, J.J.; Mendoza Fandiño, J.M.; Tavera Quiroz, H.C. Management of Natural Gas Consumption during the Manufacturing of Lead-Acid Batteries. *Sustainability* **2023**, *15*, 12030. <https://doi.org/10.3390/su151512030>

Academic Editors: Nuno Ricardo Pais Costa, Martín Tanco Rainusso and Paulo Miguel Marques Fontes

Received: 7 March 2023

Revised: 27 April 2023

Accepted: 19 May 2023

Published: 5 August 2023



**Copyright:** © 2023 by the authors. Licensee MDPI, Basel, Switzerland. This article is an open access article distributed under the terms and conditions of the Creative Commons Attribution (CC BY) license (<https://creativecommons.org/licenses/by/4.0/>).

## 1. Introduction

The current environmental situation and the energy crisis drive the pressing demand to improve energy efficiency [1] and reduce dependence on fossil fuels [1]. Globally, manufacturing accounts for over 30% of the primary energy demand and over 38% of carbon emissions [2]. Specifically, manufacturing lead-acid batteries (LAB) is energy-intensive [3,4] and has several environmental impacts, partly driven by the process energy [5,6]. LABs are projected to be the main alternative for lighting, starting, and ignition batteries for vehicles in the transport sector until 2030 [7,8]. In China, the highest producer and consumer of LABs worldwide, the environmental impacts of energy during the life cycle of LABs increased between 1990 and 2016 [9]. However, the discussion of the environmental impacts of LABs focuses on lead pollution and its health effects [6,9].

On average, LAB manufacturing demands 6.7 to 16.6 MJ/kg<sub>battery</sub> [10,11], of which electricity accounts for 65% [12] to 71.6% [13]; the heat demand (for lead refining and casting, lead oxide (PbO) powder production, grid manufacturing, curing, etc.), represents the remaining 28.4% to 35%. In China, despite the energy used per t of LAB manufactured reducing by 13% between 1990 and 2016, the total energy demand increased by 120%, driven by rising demand [9]. Therefore, the energy demand for LAB manufacturing increased about nine times faster than the manufacturing energy efficiency. Moreover, greenhouse

gas emissions from LAB manufacturing are estimated at  $1.1 \text{ kg}_{\text{CO}_2\text{eq.}}/\text{kg}_{\text{battery}}$  [4]. GHG emissions in LAB manufacturing mainly stem from lead recycling (i.e., refining and production of lead and lead alloys) because of the fuel demand [14]. LABs account for a higher impact on global warming potential than lithium and nickel alternatives [15]. Overall, GHG emissions are highly dependent on energy consumption and efficiency in LAB production [16]. Thus, higher energy efficiency standards are instrumental in reducing energy consumption and the associated economic and environmental costs. Reducing energy costs is instrumental for competitive manufacturing [17]. In industry, energy efficiency and management strategies effectively mitigate environmental impacts such as global warming and climate change while reducing energy costs [2]. However, energy management strategies are frequently misused or implemented incompletely in manufacturing [2,18].

LAB manufacturing uses fuel in crucibles, furnaces, grid-casting machines, and other technologies to produce the heat demanded by different processes. Some battery plants are using outdated technologies without adequate maintenance, which impacts the technical state and efficiency of the equipment. However, limited technical knowledge and the lack of expertise to identify inefficiencies usually prevent higher efficiency standards. More efficient technologies could improve energy efficiency by more than 20% in small and medium-sized enterprises [19]. However, this is usually difficult [4] and is mainly precluded by economic barriers [20]. Moreover, energy efficiency and management strategies are considered to be both the best and the least capital-intensive path to energy efficiency [19], with the potential to improve energy efficiency by up to 25% [21] and reduce production costs by 10 to 20% [17]. Therefore, introducing energy efficiency strategies is essential for a competitive industrial sector, rather than acquiring new technology. Improving technology management of LAB manufacturing reduces the environmental impacts [9]. However, barriers including limited access to capital [22], lack of motivation, limited technical knowledge, and lack of expertise to identify energy-saving potentials [23] have precluded higher efficiency standards in the industry. LAB manufacturing requires more research and development to implement energy efficiency standards [24].

While the energy efficiency and management of LAB manufacturing are paramount to lowering production costs [25,26], there is little discussion in the specialized literature. Most studies discussing the manufacturing of LABs focused on improving issues such as the battery charge and discharge processes, performance, longevity, and capacity of LABs [9]. The available studies that discuss the energy consumption of LAB manufacturing focus on the management and efficiency of electricity consumption during battery formation [3], the production and consumption of compressed air [27], and the battery plants [4,16]. However, to the authors' best knowledge, fuel consumption to support the heat demand required in LAB manufacturing is not discussed in the literature. Therefore, this study aims to assess the use of natural gas consumption during LAB manufacturing in order to identify saving potentials and define efficiency standards.

The novelty of this study is the assessment of the consumption and use of heat during LAB manufacturing. Additionally, it proposes efficiency indicators and highlights fuel-saving opportunities based on the use of these indicators.

## 2. Energy Management

The ISO 50001 standard [28] guides implementing, maintaining, and improving EM systems. The standard indicates using Energy Baselines (EnB) and Energy Performance Indicators (EnPI). The ISO 50001 approach is used in this case to assess the natural gas consumption in the battery plant:

1. Energy audit (to measure natural gas consumption and identify saving opportunities).
2. Implement EM strategies to improve and maintain energy efficiency standards.

During the energy audit, the gas demand and heat and combustion losses of the different processes in the plant were determined. Energy loss related to the idle operation and lead recirculation due to quality issues were also determined.

Considering the characteristics of thermal processes, the use of thermal efficiency indicators (i.e., based on energy and exergy) was considered with the energy baseline and the statistical EnPIs approach suggested by the ISO 50006 standard [29]. Exergy assessment can quantify energy systems' performance, contributing to reducing inefficiencies and pollution in energy systems [30].

Moreover, to systematize the saving opportunities identified and maintain high energy efficiency standards during the manufacturing of LABs, this study uses the general manufacturing EM framework depicted in [2]. The EM framework includes two dimensions. One dimension comprises the key components for EM (i.e., measurements, key performance indicators (KPIs, referred to as EnPIs in this study), monitoring, and evaluation and control). Moreover, the second dimension focuses on the plant operational levels (i.e., enterprise, site, area, etc.). Therefore, EM systems are applied at different levels, including [4]:

- Factory (level 1): group of process chains supported by technical services supplying the required resources.
- Process chain (level 2): distinct logical combination of machine tools for the production units/lines.
- Machine tool (level 3): unit operation and auxiliary equipment of production units/lines where operational activities occur.

When defining EnPIs, correlations of the energy baseline (EnB) of  $R^2 > 0.6$  are regarded as potential explanatory indicators, whereas correlations with  $R^2 > 0.8$  are considered potentially strong indicators [31]. Thermal efficiency and specific energy consumption (SEC) indicators can also be used as EnPIs.

Using EnPIs and EnBs, the cumulative sum chart (CUSUM) can be applied to detect deviations from the expected energy performance. CUSUM allows identification as to when interventions to address inefficiencies are needed [32]. The CUSUM, in this case, compares the expected energy consumption (based on the EnB) with the measured consumption. Moreover, to define control limits for the CUSUM chart, historical data and the Hampel identifier are used to define the median absolute deviation (MAD) [33]:

$$\text{MAD} = 1.4826 \cdot \text{median} \cdot \{|x_i - x^*|\} \quad (1)$$

where  $x^*$  is the median of the data sequence and  $x_i$  is a specific value in the data sequence ( $x_1, x_2, \dots, x_i$ ).

The EnBs defined in the sections are used to compare the evolution of their fuel consumption in different periods:

$$\text{FP}(\%) = \frac{\sum_j (F_M - F_B)}{\sum_j (F_B)} \cdot 100 \quad (2)$$

FP—Fuel performance (%)

$F_M$ —Fuel consumption measured per shift/batch

$F_B$ —Expected fuel consumption per shift/batch calculated with the EnB

$j$ —Data sequence of shifts/batches (1, 2, . . . ,  $j$ ) measured

Equation (2) is a summation from 1 to the  $j$  shift/batch on the period considered. The equation shows the percentage of fuel overconsumed or saved (i.e., the difference between measured and baseline fuel consumption). The FP can be used to assess the fuel consumption in a section over a period or to compare the performance over different periods.

### LAB Manufacturing

Battery manufacturing is a complex process that requires different steps. Figure 1 shows the process of battery manufacturing.

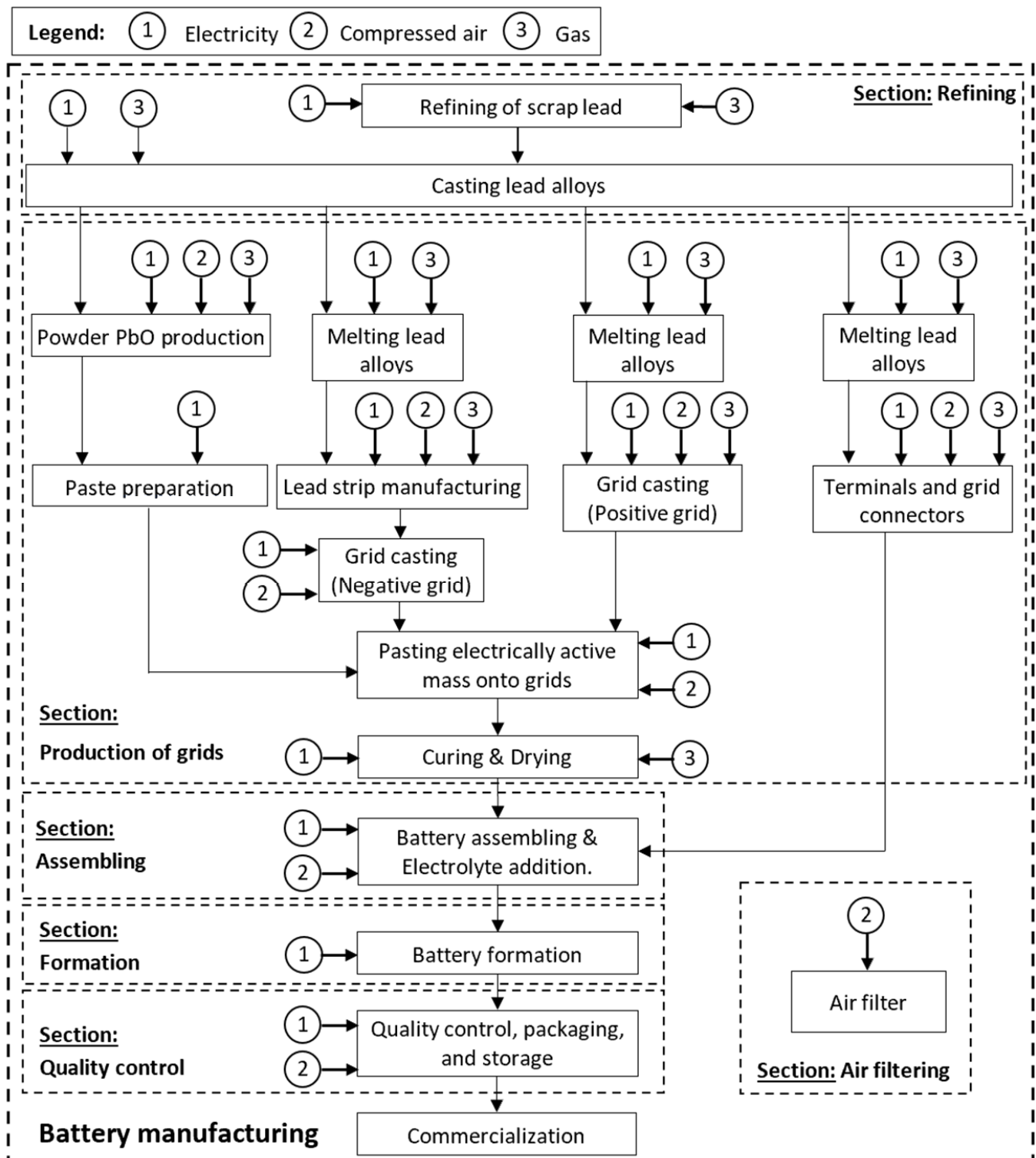


Figure 1. Process flow for lead-acid battery manufacturing (Source: adapted from [27].)

LAB manufacturing begins in the refining section, where scrap lead and ores are refined to obtain the required pure lead and lead alloys. The refined lead is then cast into ingots for storage. The active electric mass used in negative and positive grids requires leady oxide powder (PbO) paste, produced using pure lead ingots that are melted in a crucible. Similarly, lead alloys (melted in different crucibles) are used to produce the positive and negative grids, terminals, and connectors in different processes. Next, the

PbO electric active mass is pasted into the positive and negative grids, which are then dried and cured to obtain a strong porous mass skeleton bound to the grid. The different components are welded and assembled into a LAB in the assembling section, after which the electrolyte (sulfuric acid) is added, and batteries are sent to the formation process. During the formation process, batteries are charged for the first time while transforming the grids into positive and negative electrodes. Finally, formed batteries pass the quality control process and are packed and stored before commercialization. The air-filtering system uses fabric filter systems with pulse-jet cleaning to guarantee adequate indoor air quality by removing the particulate matter emitted in different processes from the air.

The heat required for refining scrap lead, melting pure lead and alloys, and drying and curing the positive and negative grids is supported by combusting different fuels (e.g., natural gas, fuel oil).

### 3. Materials and Methods

Gas flowmeters (Katronic KATflow 180 [34]) were installed in the different sections of the plant, measuring gas consumption per section for seven months, synchronized with the plant gas meter already in place, to segregate the consumption within the plant. The temperature field of different surfaces in grid casting machines and crucibles as well as the O<sub>2</sub> in combustion gases were monitored during the measuring period to check that operating conditions remained stable during the measuring period. The surface temperature was measured with a thermographic camera (FLIR E 53, Teledyne FLIR LLC, Nashua, NH, USA [35]) and the fraction of O<sub>2</sub> in combustion gases was measured with a Testo 340, Testo SE & Co. KGaA, Titisee-Neustadt, Germany [36].

#### 3.1. Production Lines

The main production lines in the plant include grid production systems, lead refining, and lead oxide powder production. Figure 2 depicts the production lines.

Scrap lead is refined in two crucibles during the refining section (see Figure 2a) in order to produce the pure lead and lead alloys needed for battery manufacturing. The crucibles are fed with lead scrap using refiners to remove Cu, Sn, Sb, and other pollutants to produce the pure lead (for lead oxide powder production) and lead alloys required for positive and negative grids, terminals, and connectors. This process is developed in several stages [37]:

1. Copper removal.
2. Softening process to remove arsenic, antimony, tin, and other elements by oxidation.
3. Removal of silver, gold, and zinc excess with the Parkes (desilverizing) process.
4. Removal of bismuth in a process similar to desilverizing.
5. Caustic clean to remove any trace impurity of antimony, calcium, magnesium, and zinc remaining from the previous processes.

Moving from one stage to the next is defined based on the laboratory results of samples taken after each stage.

Moreover, a Barton process (see Figure 2b) produces lead oxide powder in the plant. This process uses gas to melt pure lead in a crucible and feed the Barton process. Finally, positive grid manufacturing (see Figure 2c) is developed in a crucible and grid casting machines system. The plant has four positive grid production systems (i.e., one crucible feeding molten lead to two casting machines). Different molds are available in casting machines to produce the different types of positive grids needed for the different battery models manufactured in the plant. One of the grid production systems, used as a backup in case of failure or maintenance of other operational machines, has only one operating casting machine, for a total of seven casting machines.

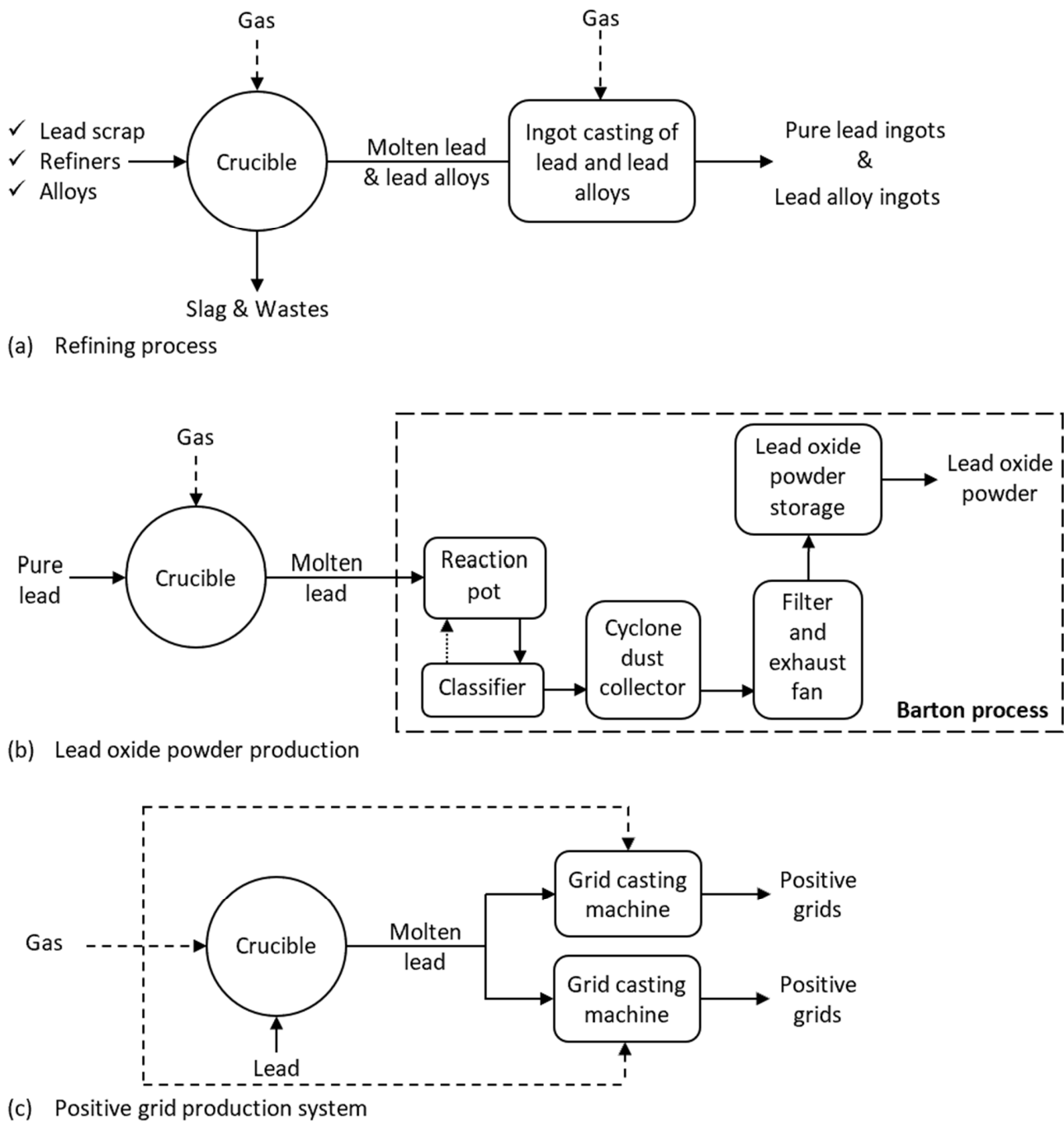


Figure 2. Process flow of the main production lines.

### 3.2. Equipment

This section describes the highest gas consuming equipment used in the plant, including the traditional crucible, the ingot casting machine, and the grid casting machine (see Figure 3).

Traditional crucibles (see Figure 3a), in which combustion gases have low residence times, operate with a thermal efficiency varying from 7 to 19% [38–40]. Other crucible designs increase the residence time of gases or introduce exhaust heat recovery systems to increase thermal efficiency by up to 28% [41]. Moreover, electric furnaces have efficiencies between 57% and 75% [42,43]. Some crucibles are entirely or partially buried in the plant, so there are no surfaces exposed to the air. Thus, no heat is lost by surface convection in those cases.

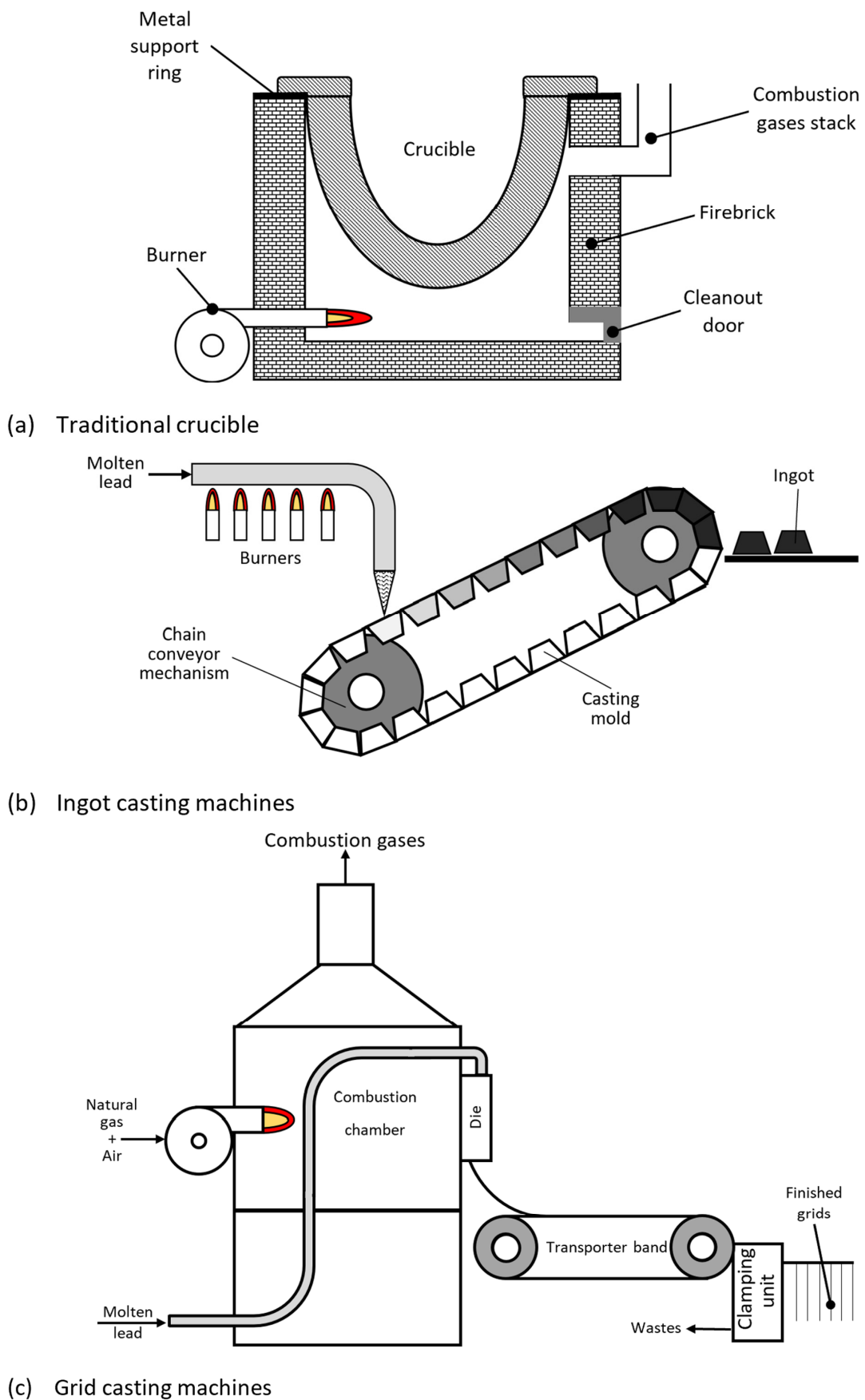
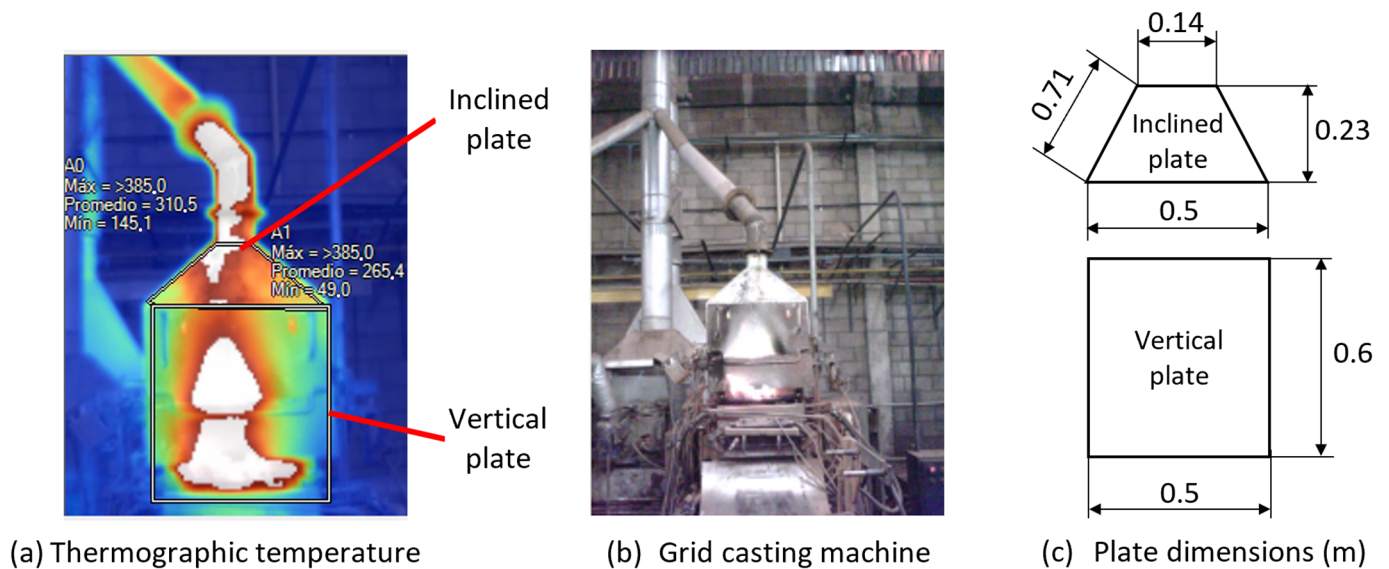


Figure 3. Main characteristics of gas-consuming systems.

The refined lead and lead alloys must be cast into ingots, for which a casting ingot machine is used. The ingot machine (see Figure 3b) has a chain conveyor mechanism that moves casting molds. The molten lead is heated using burners (or other systems) and it is poured into the casting mold during the movement of the conveyor. The metal is cooled using air and water as they move in the conveyor chain. The solid ingot is extracted once it is cold. Refining crucibles produce molten lead at temperatures between 370 and 430 °C, while casting requires temperatures ranging from 455 to 540 °C [44]. In the plant, lead is pumped from the crucible to the ingot casting machine through a pipe 2.5 m long and 0.15 m in outer diameter. The flow of lead averages 1.65 kg/s, while the average power supply of natural gas equals 364 kW.

Natural gas is combusted to melt lead ingots in a crucible and to keep lead at the required temperature during the positive grid casting process (see Figure 3c). The grid casting machine receives the molten lead from a crucible. Then, a burner is used to heat the molten lead to the required temperature before it is supplied to the die-casting unit, where grids are cast. The casted grids are dropped into a transporter band, moving grids to the clamping unit that trims the excess lead remaining from casting. The lead wasted in the clamping unit is melted again in the crucible. Moreover, the finished grids are accumulated and eventually stacked to continue the production flow. Grid-casting machines lose heat through the walls, as shown in Figure 4.



**Figure 4.** Characteristics and thermographic study of the grid casting machine.

The figure shows an average surface temperature of 265.4 °C for the vertical plate and 310.5 °C for the inclined plate. These surface temperatures represent an energy loss and a security hazard for the operators of the grid machines.

### 3.3. Combustion Analysis

The combustion excess air coefficient is calculated like [45]:

$$\lambda = 1 + \frac{O_2}{21 - O_2} \quad (3)$$

where:

$O_2$ —Percent of oxygen in the combustion gases (%).

$\lambda$ —Excess air coefficient.

The potential savings from improving combustion efficiency can be estimated from the available heat chart [46,47].

The composition of natural gas is depicted in Table 1.

**Table 1.** Composition of natural gas.

Component	Mass Fraction (%)
CH <sub>4</sub>	96.3
N <sub>2</sub>	2.6
CO <sub>2</sub>	0.4
C <sub>2</sub> H <sub>6</sub>	0.5
C <sub>3</sub> H <sub>8</sub>	0.1
C <sub>4</sub> H <sub>10</sub>	0.1
Total	100.0

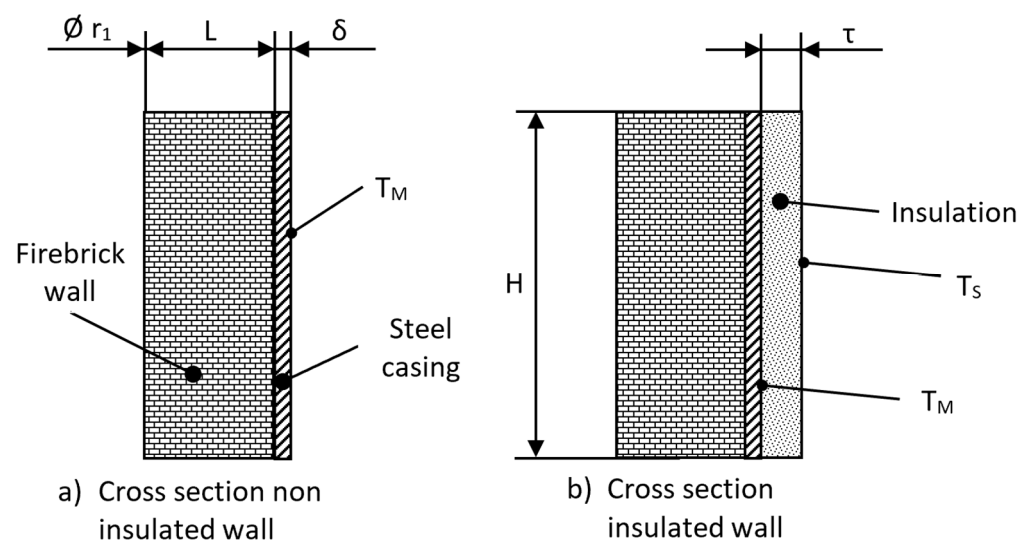
Based on the components depicted in Table 1, the stoichiometric combustion air amounts to 16.7 kg<sub>air</sub>/kg<sub>natural.gas</sub> (i.e., 11.1 kg<sub>air</sub>/m<sup>3</sup><sub>natural.gas</sub>).

### 3.4. Heat Transfer Analysis

The convection heat transfer coefficient of hot surfaces is calculated to determine the heat lost through the walls in the grid casting machines and crucibles. When necessary, adequate insulation is considered to calculate potential energy savings.

The average surface temperature is used to calculate the heat loss by convection with and without insulation.

The walls of crucibles include firebricks and a steel casing, as depicted in Figure 5.

**Figure 5.** Characteristics of the cylinder wall of crucibles for the conduction heat transfer analysis.

The figure shows the wall of crucibles built with a layer of firebricks and a steel reinforcement covering the firebricks (see Figure 5a). In this case, heat losses through the walls can be significant. Thus, insulation might be indicated (see Figure 5b). The average surface temperature measured in the equipment ( $T_M$ ) is used as a reference to calculate heat losses and energy-saving potentials. Equation (4) (without insulation), Equation (5) (plane wall with insulation), and Equation (6) (cylinder wall with insulation):

$$q_{\text{wall}} = h_{\text{out}} \cdot A_{\text{out}} \cdot (T_M - T_o) \quad (4)$$

$$q_{\text{wall}} = k_{\tau} \cdot A_{\text{out}} \cdot \frac{(T_M - T_s)}{L} = h_{\text{out}} \cdot A_{\text{out}} \cdot (T_s - T_o) \quad (5)$$

$$q_{\text{wall}} = 2 \cdot \pi \cdot k_{\tau} \cdot L \cdot \frac{(T_M - T_s)}{\ln\left(\frac{r_4}{r_3}\right)} = h_{\text{out}} \cdot A_{\text{out}} \cdot (T_s - T_o) \quad (6)$$

where:

$q_{\text{wall}}$ —Heat transfer through the wall (W)

$h_{\text{out}}$ —Convection heat transfer coefficient of the exterior surface  $\left(\frac{\text{W}}{\text{m}^2 \cdot \text{K}}\right)$

$A_{\text{out}}$ —Exterior surface ( $\text{m}^2$ )

$T_M$ —Average surface temperature measured ( $^{\circ}\text{C}$ )

$T_S$ —Surface temperature of the insulation ( $^{\circ}\text{C}$ )

$T_o$ —Ambient temperature ( $^{\circ}\text{C}$ )

$k_{\tau}$ —Thermal conductivity of the insulation material  $\left(\frac{\text{W}}{\text{m} \cdot \text{K}}\right)$  The energy-saving potential from insulating the wall is calculated considering the heat conduction and convective heat transfer through the insulating material. The use of a commercial wool ( $k_{\text{wool}} = 0.034 \frac{\text{W}}{\text{m} \cdot \text{K}}$ ) with a cost of 10.8 USD per sheet (i.e., Length = 120 cm, Width = 60 cm, Thickness = 5.08 cm) was considered for insulation [48].

The different radii of the crucible wall are calculated based on the inner radius ( $r_1$ ) of the firebrick wall as follows:

$$r_2 = r_1 + L \quad (7)$$

$$r_3 = r_2 + \delta \quad (8)$$

$$r_4 = r_3 + \tau \quad (9)$$

where:

$r_1$ —inner radius of the firebrick wall

$r_2$ —outer radius of the firebrick wall

$r_3$ —outer radius of the steel reinforcement

$r_4$ —outer radius of the insulation

The convection coefficient  $h_{\text{out}}$  is calculated as:

$$h_{\text{out}} = \frac{\text{Nu} \cdot k_{\text{aire}}}{D} \quad (10)$$

The Nusselt number for vertical plate surfaces can be calculated using Equation (10), which is suitable for most engineer calculations of vertical and inclined plates [49–51]. In the case of inclined plates,  $g$  is replaced by  $g \cdot \cos(\phi)$  to calculate  $\text{Ra}_L$  (where  $\phi$  is the inclination angle of the plate):

$$\text{Nu} = \left\{ 0.825 + \frac{0.387 \cdot \text{Ra}_L^{1/6}}{\left[ 1 + \left( \frac{0.492}{\text{Pr}} \right)^{9/16} \right]^{8/27}} \right\}^2 \quad (11)$$

where:

$\text{Nu}$ —Nusselt number  $\left(\text{Nu} = \frac{h_{\text{out}} \cdot D}{k_{\text{aire}}}\right)$

$\text{Ra}_L$ —Rayleigh number  $\left(\text{Ra}_L = \frac{g \cdot \beta \cdot (T_S - T_o) \cdot L^3}{\nu \cdot \alpha}\right)$

$T_S$ —Surface temperature

$T_o$ —Ambient temperature

$\text{Pr}$ —Prandtl number  $\left(\text{Pr} = \frac{\nu}{\alpha}\right)$

For the surface of vertical cylinders, the Nusselt number is calculated as follows [49,52–54]:

$$\text{Nu} = \frac{4}{3} \cdot \left[ \frac{7 \cdot \text{Ra} \cdot \text{Pr}^2}{5 \cdot (20 + 21 \cdot \text{Pr})} \right]^{\frac{1}{4}} + \frac{4 \cdot (272 + 315 \cdot \text{Pr}) \cdot H}{35 \cdot (64 + 63 \cdot \text{Pr}) \cdot D} \quad (12)$$

The energy-saving potentialities are calculated as the difference between the heat loss through the walls without insulation ( $q_n$ ) and the heat loss with insulation ( $q_{ideal}$ ):

$$\dot{Q}_{wall} = (q_n - q_{ideal}) \cdot t \quad (13)$$

where  $t$  is the time frame considered for the calculations.

### 3.5. Energy and Exergy Balances

The mass, energy, and exergy balances of the equipment are used to calculate the thermal efficiency. For these calculations, it is considered that the systems operate under steady-state conditions.

For an open system operating under steady-state conditions, the mass balance is given by:

$$\sum_i \dot{m}_{in} = \sum_i \dot{m}_{out} \quad (14)$$

where:

$\dot{m}_{in}$ —Input flows

$\dot{m}_{out}$ —Output flows.

The energy balance is given by:

$$iE_{in} = jE_{out} \quad (15)$$

where:

$E_{in}$ —Input energy flows

$E_{out}$ —Output energy flows.

The energy of a flow is calculated as follows:

$$\dot{E} = \dot{m} \cdot c_p \cdot \Delta T \quad (16)$$

where:

$c_p$ —Specific heat

$T$ —Temperature of the flow.

The exergy balance of a thermal system is calculated as follows:

$$\sum_i X_{in,i} = \sum_j X_{out,j} + X_D \quad (17)$$

where:

$X_{in}$ —Exergy of the input flows

$X_{out}$ —Exergy of the output flows

$X_D$ —Exergy destruction

The exergy of a flow equals:

$$X = X^{Ph} + X^{Ch} \quad (18)$$

$X^{Ph}$ —Physical exergy

$X^{Ch}$ —Chemical exergy.

The physical exergy is calculated as follows:

$$X^{Ph} = \dot{m} \cdot [(h - h_o) - T_o \cdot (s - s_o)] \quad (19)$$

where:

$h$ —Enthalpy

$S$ —Entropy

$o$ —Refers to the reference environment

The specific chemical exergy of a gas mixture is given:

$$x^{\text{Ch}} = \sum_k z_k \cdot x_k^{\text{Ch}} + R \cdot T_0 \sum_k z_k \cdot \ln(z_k) \quad (20)$$

The chemical exergy of substances was obtained from the chemical exergy calculator [55].

The exergy of the heat is given by:

$$x_Q = \left(1 - \frac{T_0}{T}\right) \cdot Q \quad (21)$$

The exergy efficiency ( $\eta_x$ ) is expressed as:

$$\eta_x = \frac{P}{F} \quad (22)$$

where:

P—Exergy product

F—Exergy input

### 3.6. GHG Emissions from the Combustion of Natural Gas

The potential reduction of GHG emissions related to the energy-saving potentials is calculated as follows:

$$\text{GHG}_{\text{mitigation}} = \text{NG}_{\text{savings}} \cdot \text{EF}_{\text{GHG}} \quad (23)$$

where  $\text{GHG}_{\text{mitigation}}$  stands for the potential reduction of GHGs associated with the potential savings of natural gas ( $\text{NG}_{\text{savings}}$ ) and  $\text{EF}_{\text{GHG}}$  stands for the GHG emission factor of natural gas.

The emissions of GHGs from natural gas in Colombia are described by UPME [56], as shown in Table 2. The equivalent emission factors are provided by [57].

**Table 2.** Equivalent GHG emissions from natural gas.

GHG	Emission (kg/TJ)	Emission Factor (kgCO <sub>2eq</sub> /kg)	Equivalent Emission (kgCO <sub>2eq</sub> /TJ)
CO <sub>2</sub>	55,540	1	55,540
CO	3.28	3	10
CH <sub>4</sub>	1	28	28
N <sub>2</sub> O	0.1	265	27
Total	-	-	55,605

In total, CO<sub>2</sub> accounts for most of the GHG emissions resulting from the combustion of natural gas. Other gases, including CO, CH<sub>4</sub>, and N<sub>2</sub>O, have marginal contributions. These emissions are equivalent to 0.2 kgCO<sub>2eq</sub> per kWh. Moreover, GHG emissions from electricity account for 0.166 kgCO<sub>2eq</sub> per kWh [58].

## 4. Results

A battery plant in Colombia using natural gas to support its heat demand is selected as a case study. Data from one year of operation was used in the calculations.

### 4.1. Gas Consumption during the Manufacturing of LAB

Table 3 shows the results and the Pareto of gas consumption per section in the plant.

**Table 3.** Pareto chart of gas consumption.

System	Gas (m <sup>3</sup> /Month)	Share (%)	Pareto (%)
Positive grid casting	24,255	36.9	36.9
Refining	20,347	31.0	67.9
Production of PbO	8626	13.1	81.0
Production of terminals and connectors	5409	8.2	89.2
Tunnel 1 (curing and drying)	3586	5.5	94.7
Tunnel 2 (curing and drying)	3492	5.3	100.0
Total	65,715	100.0	100.0

The results show that the positive grid casting machines, the lead refining process, and the process of PbO powder production account for 81% of the total demand for natural gas in the plant. Therefore, this study will focus on these three processes.

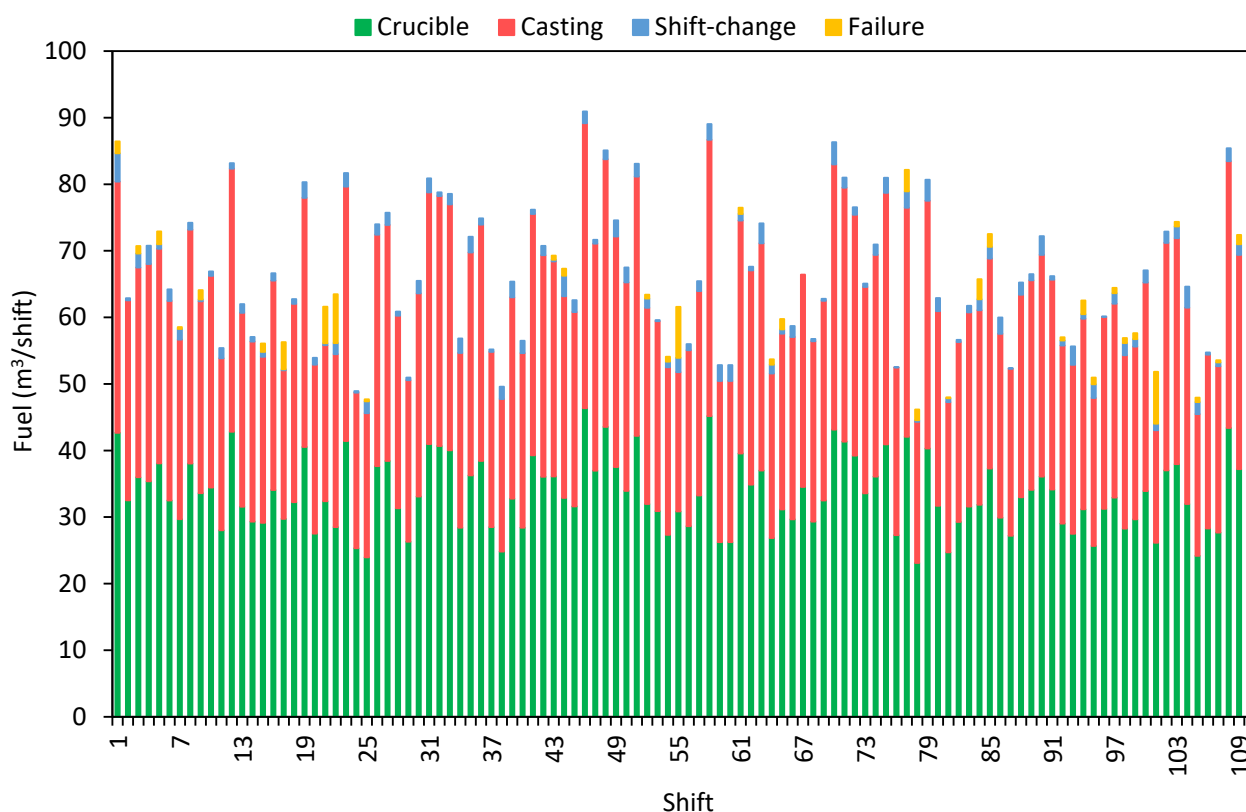
The cost of natural gas is 0.5 USD/m<sup>3</sup>, while the electricity cost is 0.15 USD/kWh.

#### 4.2. Saving Potentials

The saving potentialities are individually assessed for the systems considered in this study. Historical gas consumption and production data were only available for the refining section.

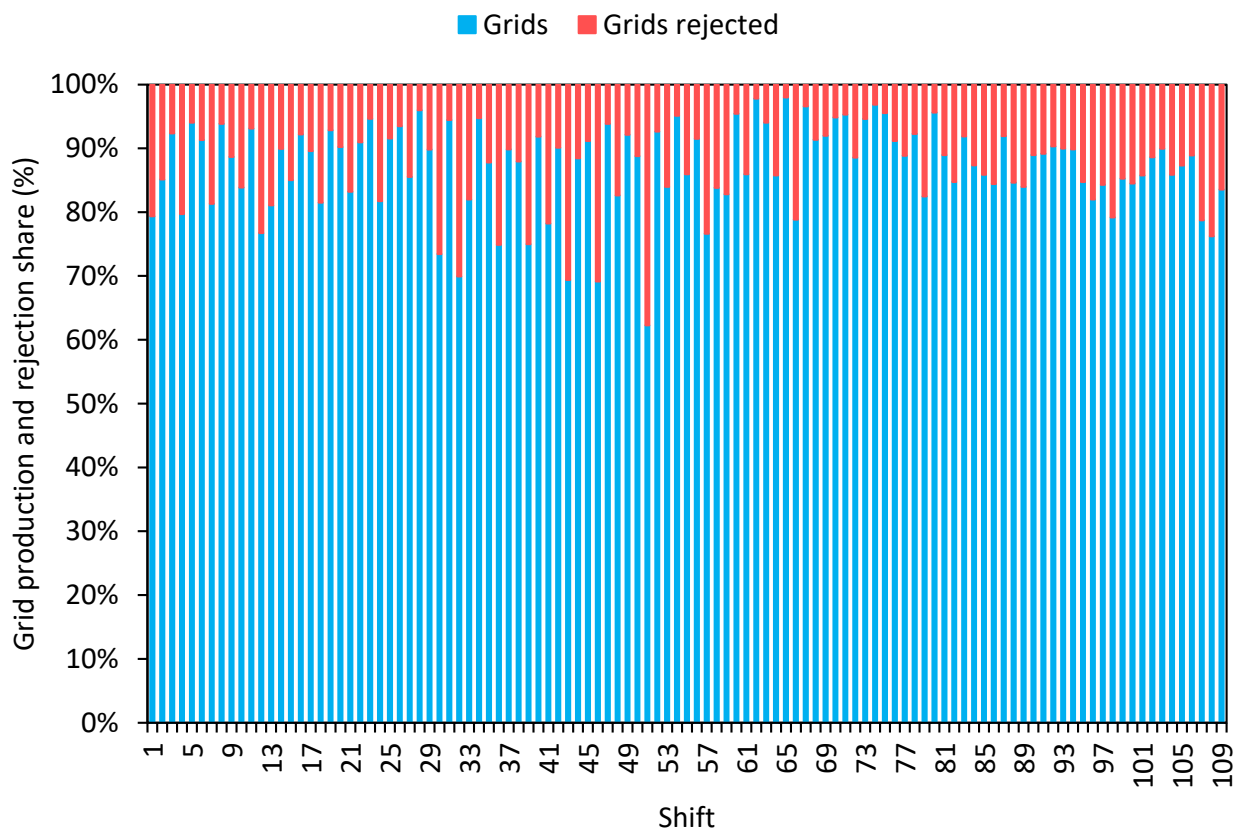
##### 4.2.1. Positive Grid Casting System

Figure 6 shows the gas consumption measured in the positive grid casting system during 109 shifts.

**Figure 6.** Gas consumption production during the operation of grid production systems.

The gas consumed during shift changes is considered a process loss (i.e., grid casting stops while gas consumption continues). Idle operation during the shift changes accounted for 3.8% of the total gas consumption, ranging from 0 to 6.9%. These results show that the change of shifts is irregular, taking different amounts of time. Moreover, when the crucible continues using fuel to keep the lead molten, idle operation during machine failures accounts for 1.6% of the production time. On average, a grid casting system uses 68.6 m<sup>3</sup> of natural gas per shift, with the crucible using 52.5% of the fuel.

Die casting units have a maximum grid casting rate regardless of the grid size (i.e., up to 10,000 grids per 8 h shift). Therefore, grid casting losses depend on the share of grids rejected. Rejected grids are mostly recirculated to the crucible, thus accounting for process inefficiency. The rate of grid rejection during grid casting varies depending on the operation of the casting machine (see Figure 7).



**Figure 7.** Grid rejection rate in the casting units.

On average, around 13% of the grids produced during a shift are rejected, varying between 2 and 38%. About 10% of the shifts measured operate with grid rejection rates lower than 5%. Moreover, lead consumption averages 764.5 kg/shift (i.e., from 241 to 1131 kg/shift), while grid production averages 731.2 kg/shift.

The relation between gas consumption and grid production is shown in Figure 8.

The figure shows no correlation between grid production and gas consumption. These differences are explained by the factors affecting gas consumption, including failures, shift change, operation of the system, etc.

The exergy efficiency of the positive grid production process is defined as the ratio of the chemical exergy of grids to the exergy input to the process (i.e., the exergy of natural gas, air, and lead).

$$\eta_x = \frac{X_{\text{Grid}}^{\text{Ch}}}{X_{\text{ingots}} + X_{\text{n.gas}} + X_{\text{air}}} \quad (24)$$

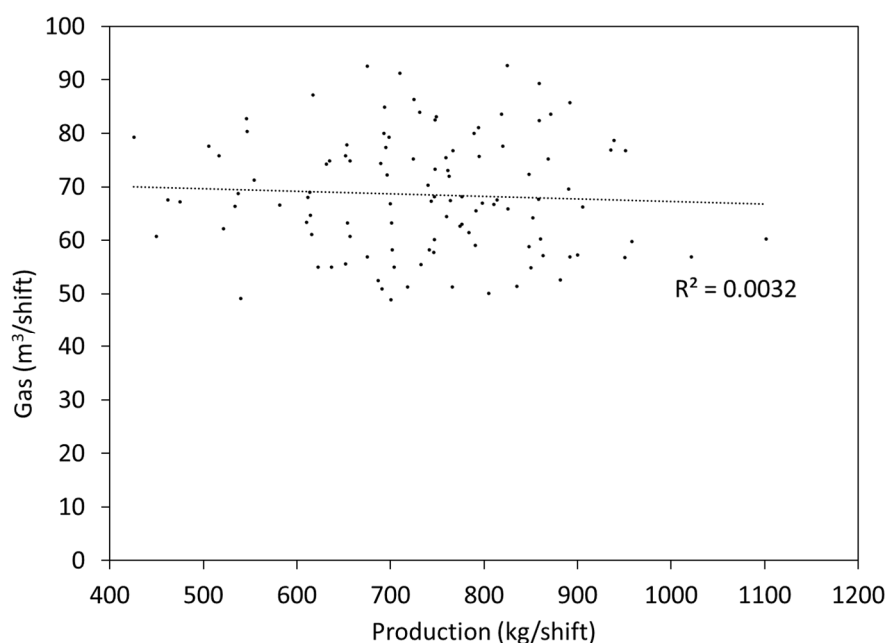


**Figure 8.** Gas consumption vs. grid production.

The exergy balance for the grid casting systems is depicted in Table 4. The exergy destruction includes the natural gas used during failures and shifts change when grid production stops while fuel is still consumed.

**Table 4.** Exergy balance of the grid casting system.

Flow	Equipment	Flow (kg/Shift)	T (°C)	T (K)	$e_{ch}$ $e_{ph}$		$E_{ch}$	$E_{ph}$	$E_T$	$E_T$ (%)
					(kJ/kg)					
Lead	Crucible	769.3	38	311	1064.5	0.0	818.9	0.0	818.9	18.1
Fuel *		38.0	38	311	38,584.0	0.0	1465.0	0.0	1465.1	32.3
Air		636.4	38	311	48.4	0.0	30.8	0.0	30.8	0.7
Molten lead		769.3	450	723	1064.5	62.9	818.9	48.4	867.2	19.1
Combustion gas		674.4	253	526	197.5	295.8	133.2	199.5	332.7	7.3
Exergy destruction		-	-	-	-	-	-	-	1039.4	24.6
Molten lead	Casting machine	769.3	450	723	1064.5	62.9	818.9	48.4	867.2	19.1
Fuel *		34.3	38	311	38,584.0	0.0	1323.6	0.0	1323.6	29.2
Air		582.6	38	311	48.4	0.0	28.2	0.0	28.2	0.6
Grids		735.8	80	353	1064.5	6.4	783.2	4.7	787.9	17.4
Grids rejected		33.5	80	353	1064.5	6.4	35.7	0.2	35.9	0.8
Combustion gas		616.9	302	575	164.4	363.3	101.4	224.1	325.5	7.2
Heat loss	-	-	-	-	-	-	-	43.9	1.0	
Exergy destruction	-	-	-	-	-	-	-	957.6	22.6	

\* Natural gas flow in m<sup>3</sup>/h.

The system uses 51% in the crucible and the remaining in the casting machine. The grid casting system operates with an overall exergy efficiency of 17.4%. Inefficiencies are explained because the crucible and casting machine irreversibly destroy 47.2% of the exergy input. The exergy destruction includes some 3.2% lost during failures and shift changes. Exergy destruction is driven by combustion and heat and by momentum transfer. Therefore, saving opportunities can be realized by improving the combustion processes, reducing the

physical exergy lost with the combustion gases and the heat loss, and minimizing losses during equipment failure and shift changes.

Figure 9 shows the correlations of the SEC and the exergy efficiency to the flow of grid production in one grid casting system.

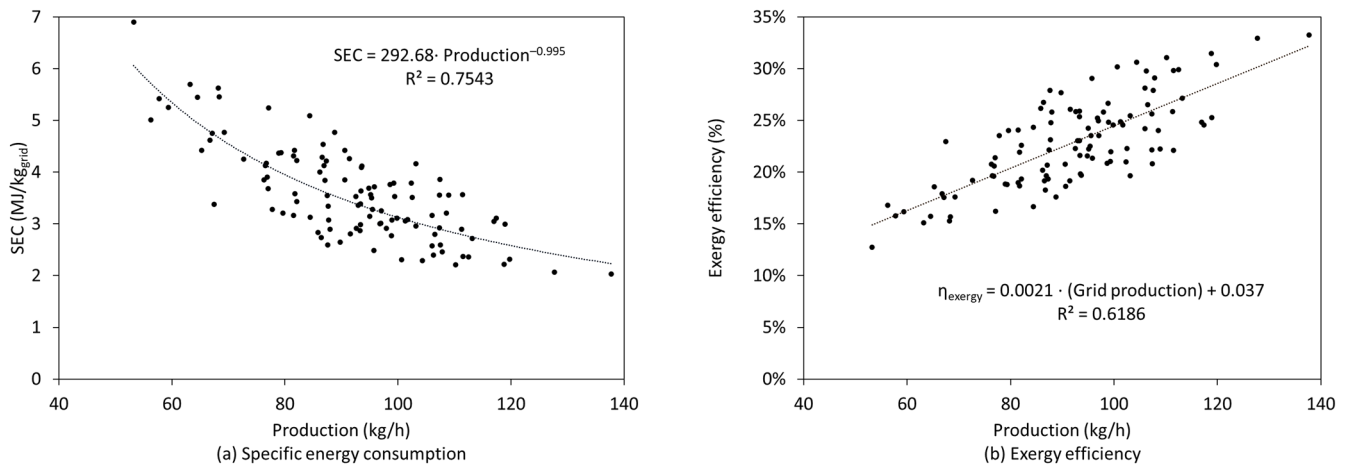


**Figure 9.** Correlations of grid production to energy parameters.

The results show that the SEC is an adequate EnPI to monitor this process. However, exergy efficiency can be used to identify process losses. The SEC with a correlation of  $R^2 > 0.6$  can be considered as a potential EnPI. In this case, the positive grid casting process operated with a FP of 6.1%.

#### 4.2.2. Refining

- A. Pure lead
- B. Lead-calcium-tin alloy for negative grids
- C. Lead-calcium-tin alloy for positive grids
- D. Lead-antimony alloy

The data for refined lead production and natural gas consumption measured in the plant is shown in Figure 10.

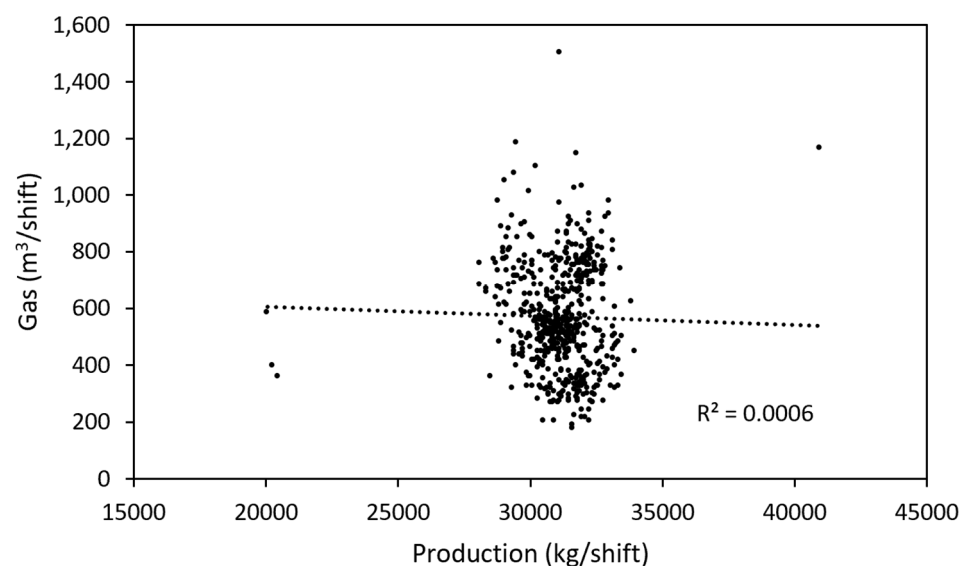


**Figure 10.** Production of refined lead vs. gas consumption (3-year data).

The figure shows no correlation between the production of refined lead and the consumption of natural gas. This is explained because the gas used for refining strongly

depends on the scrap quality used in the refining batches (i.e., refining lower scrap quality has higher energy requirements). On the other hand, reducing the delay between refining stages is possible by addressing the delay in reporting laboratory results. During this delay, crucibles use fuel to maintain the temperature of the batch, accounting for a fuel loss. Frequently (especially during the night), laboratory results are not immediately available in the refining section. On average, refining demands 558 MJ/t, while ingot casting requires 233 MJ/t (i.e., 791 MJ/t for the section). In contrast, the specialized literature reports refining crucibles and ingot casting with a total energy demand between 358.7 MJ/t (i.e., 0.34 million BTU) [58] and 276.3 MJ/t (i.e., 224.9 MJ/t for refining and 51.4 MJ/t for casting) [59]. Therefore, the energy demand measured is between 2.2 and 2.9 times higher than the demand reported in the literature for these processes [58,59]. Given the low correlation between gas consumption and refined lead production, a different EnPI is needed to assess the energy use in this process.

The exergy efficiency is an alternative EnPI used to assess the refining process. In this case, the efficiency is defined as the ratio of the chemical exergy of refined lead to the exergy input to the process (i.e., the exergy of natural gas, air, and scrap lead):

$$\eta_x = \frac{X_{\text{lead}}^{\text{Ch}}}{X_{\text{scrap}} + X_{\text{n.gas}} + X_{\text{air}}} \quad (25)$$

The mass and exergy balances of the average production in the section during the production and ingot casting of refined lead are presented in Table 5.

**Table 5.** Mass and exergy balances of the lead refining process.

Flow	Equipment	m (kg/Batch)	T (°C)	$X_{\text{ch}}$	$X_{\text{ph}}$	$X_{\text{total}}$	
				(MJ/Batch)			
Scrap		32,793	38	34,908	0	34,908	
Natural gas	Crucible	In	325	38	12,543	0	12,543
Air			5088	38	247	0	247
Refined lead			29,123	400	31,001	520	31,521
Slag			Out	3670	400	3907	66
Surface heat loss	-	160		-	375	375	
Combustion gases	5413	313		1034	492	1526	
Refined lead	Ingot	In	29,123	400	31,001	520	31,521
Natural gas			133	38	5113	0	5113
Ingots			Out	29,123	90	31,001	17

The refining process operates with an overall exergy efficiency of 58.7%. Inefficiencies are explained because 11.1% of the exergy (i.e., 5873 MJ/batch) is lost with the slag, the combustion gases, and the surface heat loss, while 30.1% of the exergy is destroyed in the crucible (i.e., accounting for 10,306 MJ/batch) and in the ingot casting system (i.e., accounting for 5614 MJ/batch). Exergy destruction is driven by the chemical reactions in the processes (i.e., combustion and refining reactions) and physical processes such as heat and momentum transfer. Exergy destruction during combustion increases with the excess air [60]. Therefore, saving opportunities can be obtained by reducing the physical exergy lost with hot gases and heat loss and improving the combustion of natural gas.

Figure 11 shows the relation of the SEC and the exergy efficiency to the flow of lead refined in the refining crucible.

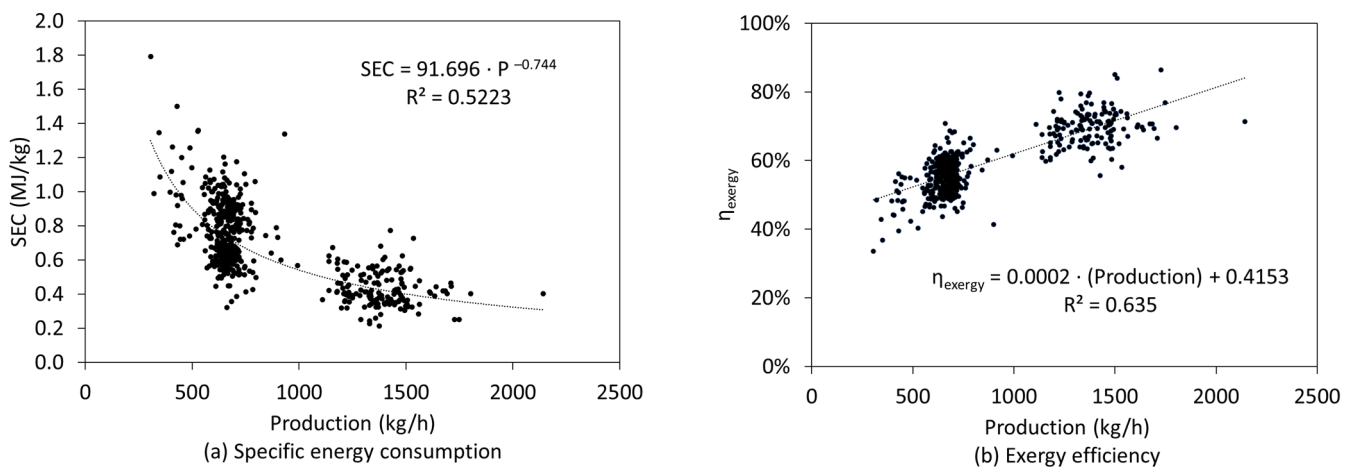


**Figure 11.** Correlations of SEC and exergy efficiency to the flow of refined lead.

The figure shows that the correlation between production and SEC is lower than indicated for an EnPI. Moreover, with a correlation of  $R^2 > 0.6$ , the exergy efficiency can be considered as a potential EnPI. Thus, it can be used to monitor and control energy use during lead refining. Based on this EnPI, energy savings can be achieved by monitoring the performance of the refining process. Contrasted to the EnB of exergy efficiency during the period considered, the refining system operated with an FP of 7.4%.

Saving opportunities were identified with the surface heat loss in the refining crucible, the excess air in the natural gas combustion in the crucible, and the lead heating system used for ingot casting. Furthermore, the time between sampling and the availability of laboratory results could be reduced, particularly during night shifts. Using natural gas in the refining crucible is strongly influenced by batch production time. Table 6 shows the natural gas consumption and saving potentials of the refining crucible. In this case, the surface heat loss was calculated using Equation (3) for the measured conditions and Equation (5) for the insulated crucible, while the convection coefficient of the crucible surface was calculated using Equation (11). Moreover, the potential savings were calculated using Equation (12), for which an average of 41 h per refining batch, operating with an excess air of 1.41, is considered. The properties of air were taken from [61].

**Table 6.** Natural gas consumption and saving potential during the operation of the refining crucible.

Parameter	Unit	Crucible Surface		
		Current	Optimized	Savings
Surface temperature	°C	159.6	80	-
Surface heat loss	W	8971	2454	6516
Excess air ( $\lambda$ )	-	1.41	1.10	-
Combustion efficiency ( $\lambda$ )	%	72.5	74.2	1.7
Natural gas	m <sup>3</sup> /batch	471.7	437.6	34.1
GHG emissions	kgCO <sub>2eq</sub> /batch	973.1	902.7	70.4
Cost	USD/batch	235.9	218.8	17.1

The average surface temperature of 159.6 °C, measured with the thermographic assessment, accounts for an energy loss and a security hazard and could be reduced to 80 °C using insulation. The use of insulation to reduce surface heat loss in the crucible could reduce the fuel demand by 5.5%. In total, 24 insulation wool sheets are needed for the crucible, requiring an investment of 259.2 USD. This investment can be recovered within 16 refining batches (i.e., around 1.5 months, considering 132 refining batches per year). On

the other hand, improving the combustion efficiency by reducing  $\lambda$  can further reduce fuel consumption per batch by 1.7%.

Furthermore, reducing the exit temperature of combustion gases to 150 °C by improving heat transfer in the crucible could reduce fuel consumption by 8.5%. However, realizing this potential is challenging at best since enhancing heat transfer between the combustion gases and the lead in the crucible requires implementing modifications or eventually replacing it. Therefore, this aspect will not be further discussed in this case. Because of the difficulties in measuring the delays in the availability of laboratory results after sampling the refining process, it was impossible to estimate saving potentials. However, reducing the time was proposed as a saving measure.

The heating system currently used in the ingot casting system accounts for the main saving potential. Heating a lead flow of 1.2 to 1.7 kg/s from 399 °C to 504 °C (values measured in the plant) requires a heat flow of 18 to 51 kW. Currently, the heating system consumes an energy flow of 306 to 562 kW (i.e., an energy efficiency of 6 to 9%). Therefore, an alternative process could be indicated to heat the lead flow to the casting temperature. The impedance pipe heating system, available for lead heating (see Figure 12), is an alternative to the current system. Impedance pipe heating systems operate with an energy efficiency ranging from 40 to over 90% [62] and are available from 1 kW to several MW to heat up to 1090 °C, with heat flows up to 29.5 W/cm<sup>2</sup> [63]. Impedance heating systems are available at capital costs of 2838 to 4118 USD per m [64,65].

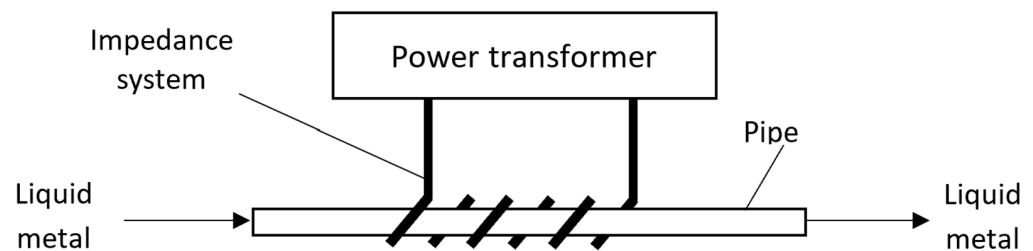


Figure 12. Impedance pipe heating system.

Heating a lead flow of up to 1.7 kg/s in an impedance pipe heating system requires a heat flow of 27 kW. Table 7 shows the saving potential for the use of an impedance heating system.

Table 7. Saving potential of impedance heating system.

Equipment	Unit	Combustion	Impedance		Savings	
			Min.	Max.	Min.	Max.
Natural gas	m <sup>3</sup> /batch	192.3	-	-	-	-
Electricity	kWh/batch	-	137.7	309.8	-	-
Energy costs	USD/batch	96.1	20.7	46.5	75.5	49.7
GHG emissions	kgCO <sub>2eq.</sub> /batch	396.7	22.9	51.4	373.8	345.2
Capital cost	USD	-	-	4118	-	-

Based on the results, the capital investment in the impedance system would be recovered in 55 to 83 refining batches (i.e., around 5 to 8 months). Thus, economically, the investment looks attractive. Moreover, GHG emissions will be reduced to 5.8 to 13.0% of the current emissions.

#### 4.2.3. Ledy Oxide Powder Production

Ledy oxide powder production is a complex process. Most of the gas consumption in this process occurs in the crucible that operates for a monthly average of 525 h to melt

the lead ingots and feed molten lead to the Barton process. Therefore, the assessment of this area focused on the crucible, which, similar to the refining crucible, shows high surface temperatures. The thermographic measures show a surface temperature varying from 100 to 241 °C, with an average of 159 °C. Figure 13 shows the relation between the produced PbO and the gas consumed in the process.

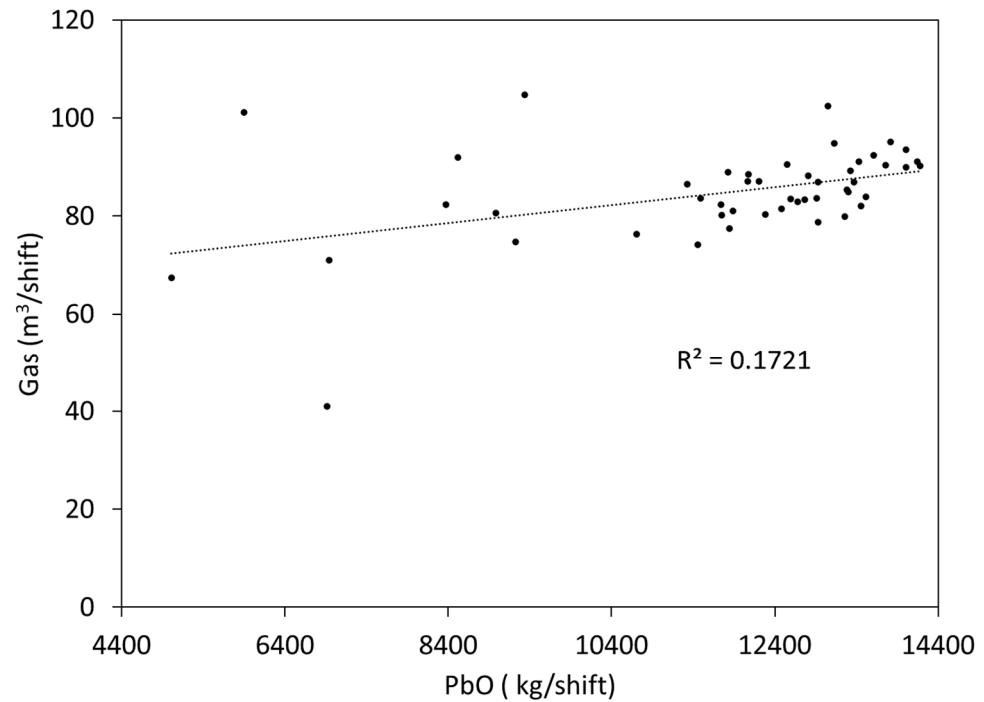


**Figure 13.** Production of leady oxide vs. gas consumption.

The results show no correlation between the production of leady oxide and gas consumption.

The exergy efficiency for leady oxide powder production is defined as the ratio of the chemical exergy of the leady oxide powder to the exergy input to the process (i.e., the exergy of natural gas, air, and lead):

$$\eta_x = \frac{X_{\text{PbO}}^{\text{Ch}}}{X_{\text{Lead}} + X_{\text{n.gas}} + X_{\text{air}}} \quad (26)$$

The mass and exergy balances of the average production in the section during the production and ingot casting of refined lead are presented in Table 8.

**Table 8.** Mass and exergy balances of the leady oxide powder production process.

Flow	Process	T (°C)	Flow (kg/h)	X <sub>ch</sub> (kW)	X <sub>ph</sub> (kW)	X <sub>T</sub> (kW)
Lead		38	957.4	283.1	0.0	283.1
Molten lead		414	957.4	283.1	8.9	292.0
Natural gas	Crucible	38	4.5	48.4	0.0	48.4
Air (combustion)		38	106.4	1.4	0.0	1.4
Combustion gases		253	110.9	1.5	2.2	3.7
Natural gas	Barton	38	0.5	5.4	0.0	5.4
Air (combustion)		38	12.6	0.2	0.0	0.2
Air (reaction)		38	124.4	1.7	0.0	1.7
Leady oxide		97	1009.5	120.5	0.4	120.9

The exergy balance shows that most of the exergy is unavoidably destroyed during the Barton process. Moreover, in the crucible, 7.6% of the fuel exergy is lost with combustion gases, while irreversibilities account for most of the inefficiencies, mainly due to the combustion and heat transfer processes.

Table 9 shows the natural gas consumption and saving potentials of the lead oxide crucible, considering the measured exit temperature of combustion gases of 250 °C.

**Table 9.** Natural gas consumption and saving potential in the operation of the PbO powder crucible.

Parameter	Unit	Crucible Surface			
		Current	Optimized	Savings	
Temperature	°C	159.3	94.5	-	
Heat loss	kW	1.55	0.61	0.94	
$\lambda$		1.5	1.1	-	
$\eta_{\text{combustion}}$	%	75.8	77.1	1.3	
Natural gas	Insulation	$\frac{\text{m}^3}{\text{month}}$	85	33	51
	Combustion		-	-	52
GHG emissions	Insulation	$\frac{\text{kg}_{\text{CO}_2\text{eq}}}{\text{month}}$	175	69	106
	Combustion		-	-	107
Cost	Insulation	$\frac{\text{USD}}{\text{month}}$	87	34	53
	Combustion		-	-	26

Results show that insulation can reduce the surface temperature to 94.5 °C, thereby reducing surface heat losses by 61%. In total, the gas consumption in the section can be reduced by 2.6% (i.e., 1.3% by insulating the crucible and 1.3% by controlling the excess air to 1.1). Insulating the crucible requires 11 wool sheets costing 119 USD. This investment can be recovered in less than three months. Moreover, reducing the exit temperature of combustion gases in the crucible to 120 °C might reduce the demand for natural gas by 6.8%; however, this improvement requires modifications to the crucible design that are challenging at best and are therefore excluded from this assessment. Finally, the gas flow in this crucible is manually controlled, and operators usually set a fixed flow during the shift, leading to inefficiencies. Controlling the fuel flow as a function of the lead temperature is more indicated and efficient.

Figure 14 shows the SEC and the exergy efficiency of lead oxide production.

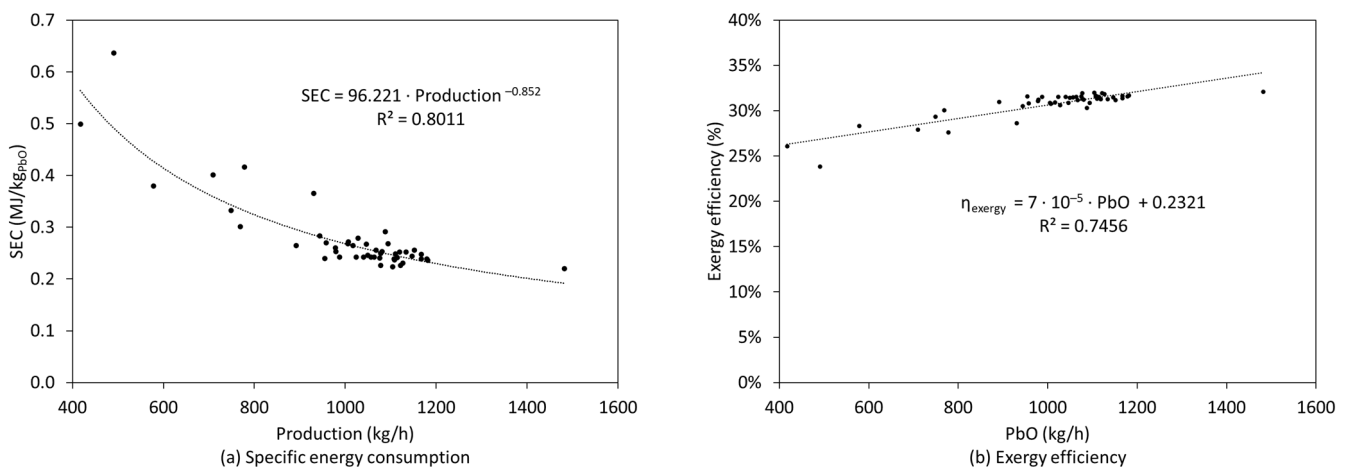


**Figure 14.** Correlations of lead oxide powder production to energy parameters.

The results show that both indicators are potential EnPIs with  $R^2 > 0.6$ . However, the SEC is a potentially strong indicator ( $R^2 > 0.8$ ). In any case, the exergy balance can be used to highlight and quantify the source of inefficiencies detected with the SEC. The results show that the system operated with an FP of 0.3%.

### 5. Implementation and Discussion

Based on the results, different saving potentialities were identified in the plant (see Figure 15).

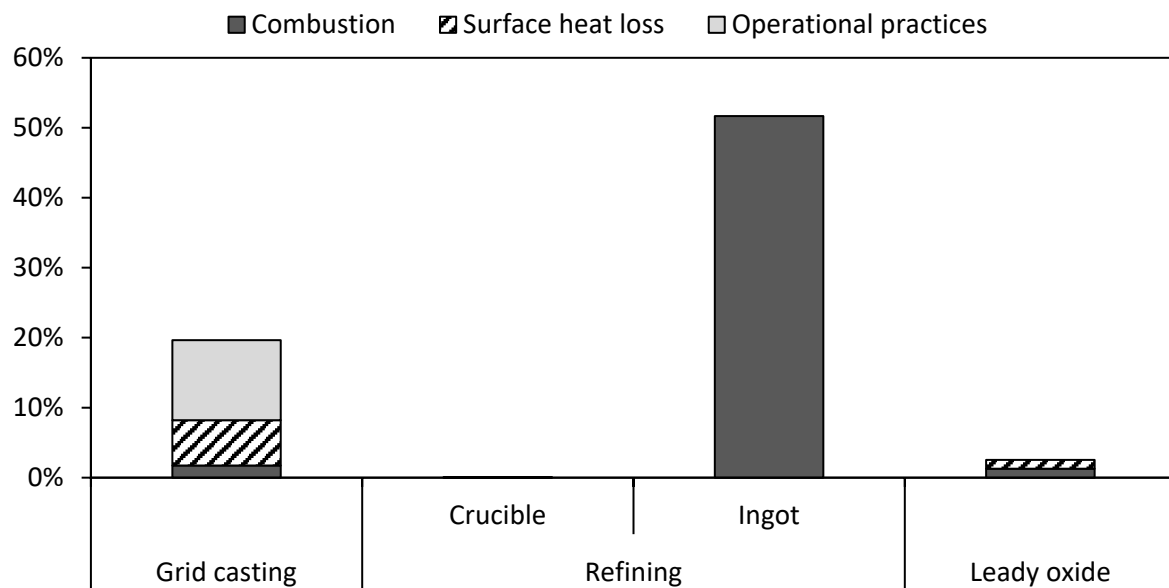


Figure 15. Saving potentials identified.

In total, the saving potential of the grid casting machines accounts for 20% of the natural gas consumption of the section, coinciding with 2.8% of the plant consumption (i.e., some 0.9% per grid casting system). In this section, improving operational practices has the highest potential. Moreover, saving potentials in the refining section crucible account for a low 0.06% of the natural gas consumption of the section, while the ingot casting system can save 52%. The saving potential in this section accounts for 13.6% of the natural gas consumption in the plant. Finally, some 2.6% of the natural gas consumption of the lead oxide production section could be saved in the crucible, which coincides with 0.1% of the plant consumption. Overall, replacing the heating system of ingot casting has the plant's highest saving potential.

Initially, measures to improve operational practices and reduce surface heat loss were implemented in different areas. Other capital-intensive and time-consuming measures requiring improving or replacing technology, such as improving combustion efficiency or replacing the ingot casting system, were postponed due to the difficulty in securing the necessary funding and organizing the processes to reduce the impact on production because of the time needed to modify or replace technology.

Figure 16 shows the results of implementing the saving measures related to improving operational practices and surface heat loss in one casting unit in the grid casting section during 30 shifts (i.e., around 15 days of operation). In this case, the EnPI used is the SEC defined in Figure 9.

The results show that improving poor operational practices and implementing insulation in the casting units permitted controlling the energy consumption within the control limits defined during the tests. The FP was reduced from 6.1% to  $-1.1\%$ , reducing fuel consumption, fuel costs, and GHG emissions by 6.8% (i.e., monthly savings of 286 m<sup>3</sup>, 143 USD, and 589 kg<sub>CO2eq.</sub>). Reducing gas consumption can be realized by expanding the

saving measures to other grid casting systems. Other improvements can be realized by improving combustion efficiency.

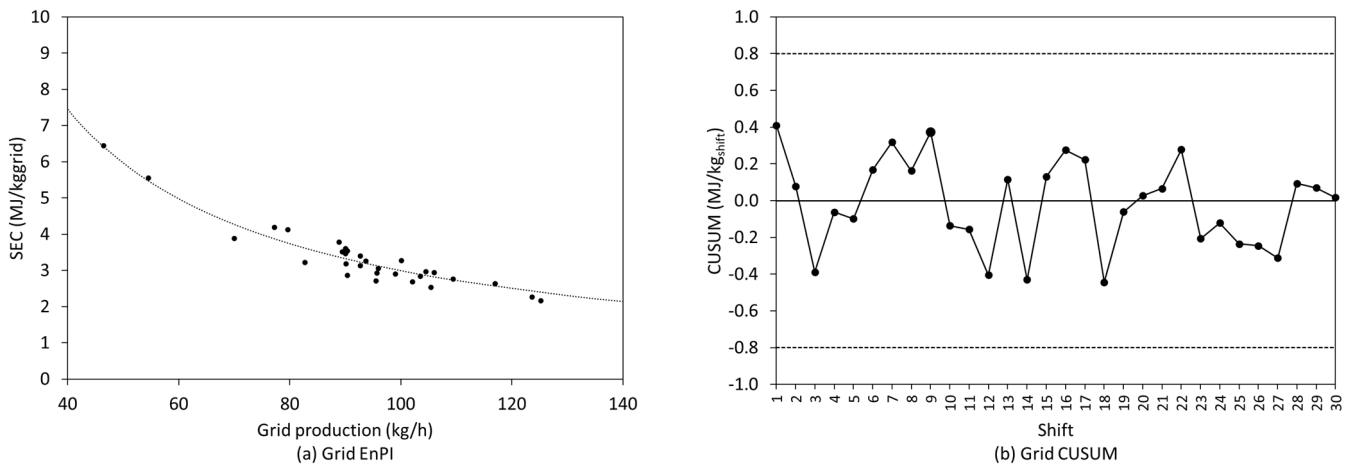


**Figure 16.** Results from implementing saving measures in the grid casting section.

Figure 17 shows the results of implementing the saving measures in the refining sections during 17 batches of lead refining (i.e., around 35 days of operation). In this case, the insulation was implemented in the crucible, and the time used in laboratory analysis was monitored. The exergy efficiency EnPI defined in Figure 11 is used in the assessment. In the event of improving or replacing the ingot casting technology in the future, the EnPI must be updated since the energy demand in the process will change significantly.

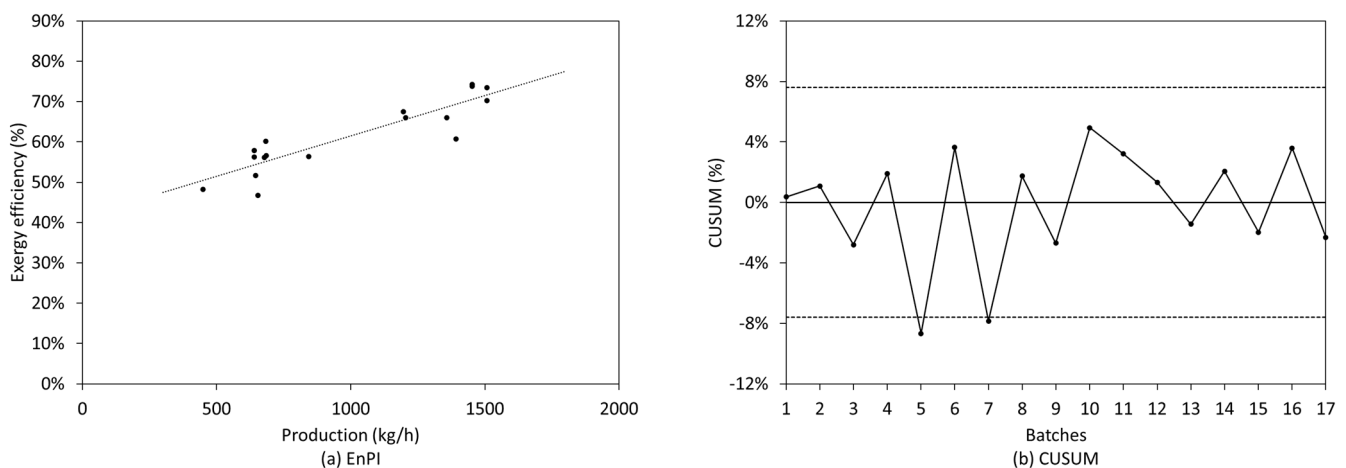


**Figure 17.** Results from implementing saving measures in the refining section.

The results show that they operated within control limits defined in 17 refining batches implementing saving measures, while two operated at efficiencies under the lower limit. In these two batches, the use of low-quality scrap was identified, which is unavoidable on occasion. Additionally, some delays were detected in the laboratory analysis used to report sampling results during the night shifts. Based on the CUSUM graph, delays were addressed after each batch, and no other incident was detected during the tests. In contrast to the baseline, the process operated with an FP of 2.2%, coinciding with savings of 476 m<sup>3</sup> of gas (i.e., savings of 4.8%), reducing emissions of GHGs by 981 kgCO<sub>2eq</sub>. The costs of natural gas are reduced by 238 USD. Monthly savings are estimated at 408 m<sup>3</sup> of natural gas (i.e., 204 USD per month) and 841 kgCO<sub>2eq</sub>.

Figure 18 shows the results of implementing the saving measures in the leady oxide powder crucible for 25 days. The SEC defined in Figure 14 was used to assess the crucible performance.

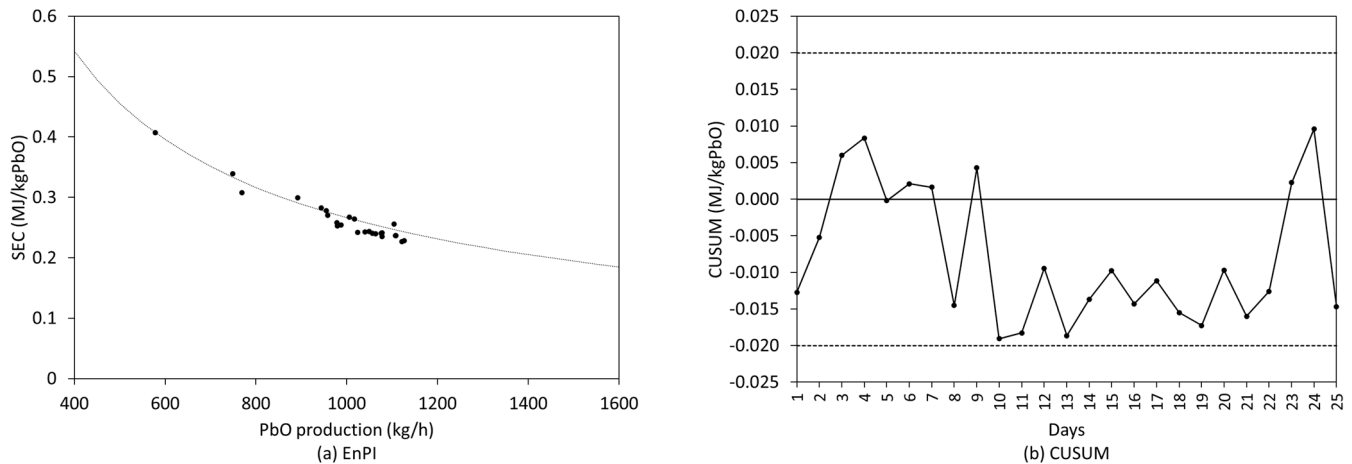


**Figure 18.** Results from implementing saving measures in the leady oxide powder production section.

The results show that during the implementation of the saving measures, the system operated within the control limits. The crucible improved its performance to an FP of  $-2.4\%$ , reducing gas consumption by  $70 \text{ m}^3$  (i.e., 35 USD) and GHG emissions by  $144 \text{ kgCO}_2\text{eq.}$  Monthly savings are estimated at  $84 \text{ m}^3$  of natural gas (i.e., 42 USD per year) and  $173 \text{ kgCO}_2\text{eq.}$

In total, saving measures led to savings of 1.2% of the natural gas consumption in the plant. These savings coincide with the emissions of  $1603 \text{ kgCO}_2\text{eq.}$  and a cost of 389 USD monthly. The operation of crucibles shows a significant gap between systems with higher residence time and heat recovery systems. Considering the low efficiency of traditional crucibles (i.e., 7 to 19% [38–40]), up to 60% of the heat lost by radiation can be reduced with either electric or induction furnaces with efficiencies between 57% and 75% [42,43]; this could reduce the natural gas demand significantly. Moreover, introducing heat recovery systems and increasing the residence time of hot gases could increase the efficiency of current crucibles. Moreover, the ingot casting system should be replaced to potentially reduce the energy costs of the process between 52 and 79%.

## 6. Conclusions

The manufacturing of lead-acid batteries is an energy-intensive process, needing significant amounts of heat. Particularly, grid casting, refining, and leady oxide production account for over 80% of the heat demand in the plant, which is mainly located on the crucibles, the grid casting units, and the ingot casting system. The highest saving potentials are identified in inefficient combustion processes, surface heat loss, and poor operational practices. Specifically, changing the ingot casting technology could save 13% of the gas consumption in the plant. Therefore, it is indicated to assess in detail the investment in a new ingot casting system.

The use of SEC and exergy efficiency indicators allow for effective monitoring and control of the performance of thermal processes in LAB manufacturing. Implementing basic saving measures to reduce surface heat loss and avoid poor operational practices resulted in estimated savings of 1.2% of the total gas consumption. By expanding the saving measures to the other grid casting units in the plant, savings can be increased to 2.1% of the plant gas consumption. The use of CUSUM within the energy management system permits the systematization of higher efficiency standards in battery manufacturing. It is recommended to assess the improvement of the current crucibles or replace them with electric or induction crucibles, and to replace the ingot casting system.

**Author Contributions:** Conceptualization, A.S.G.; methodology, A.S.G., J.J.C.E.; validation, A.S.G., J.M.M.F.; formal analysis, A.S.G., J.J.C.E.; investigation, A.S.G., J.J.C.E.; resources, J.M.M.F.; writing—original draft preparation A.S.G.; writing—review and editing, J.J.C.E., J.M.M.F., H.C.T.Q.; supervision, J.J.C.E.; project administration, J.M.M.F.; funding acquisition, J.M.M.F. All authors have read and agreed to the published version of the manuscript.

**Funding:** This research was funded by Universidad of Cordoba through the project FI-04-22.

**Data Availability Statement:** Restrictions apply to the availability of these data. Data was obtained from a battery manufacturing company and are available from the authors with the permission of the company.

**Acknowledgments:** The authors like to acknowledge the University of Córdoba and its research groups strengthening project for the support through the Framework Agreement for the mobility of students and professors between undergraduate and postgraduate academic programs from engineering faculties in higher education institutions in the Caribbean region, Colombia. Additionally, the authors like to acknowledge the support of Universidad de la Costa for the support through the investigation.

**Conflicts of Interest:** The authors declare no conflict of interest.

## References

- Caetano, B.C.; Santos, N.D.S.A.; Hanriot, V.M.; Sandoval, O.R.; Huebner, R. Energy Conversion of Biogas from Livestock Manure to Electricity Energy Using a Stirling Engine. *Energy Convers. Manag.* **2022**, *15*, 100224. [[CrossRef](#)]
- May, G.; Stahl, B.; Taisch, M.; Kiritsis, D.; Barletta, I.; Stahl, B.; Taisch, M. Energy Management in Manufacturing: From Literature Review to a Conceptual Framework. *J. Clean. Prod.* **2017**, *167*, 1464–1489. [[CrossRef](#)]
- Cabello, J.J.; Sagastume, A.; Sousa, V.; Hernández, H.; Balbis, M.; Silva, J.; Noriega, E.M.; Vandecasteele, C.; Cabello Eras, J.J.; Gutiérrez, A.S.; et al. Energy Management in the Formation of Light, Starter, and Ignition Lead-Acid Batteries. *Energy Effic.* **2019**, *12*, 1219–1236. [[CrossRef](#)]
- Gutiérrez, A.S.; Eras, J.J.; Santos, V.S.; Herrera, H.H.; Hens, L.; Vandecasteele, C. Electricity Management in the Production of Lead-Acid Batteries: The Industrial Case of a Production Plant in Colombia. *J. Clean. Prod.* **2018**, *198*, 1443–1458. [[CrossRef](#)]
- Dahodwalla, H.; Herat, S. Cleaner Production Options for Lead-Acid Battery Manufacturing Industry. *J. Clean. Prod.* **2000**, *8*, 133–142. [[CrossRef](#)]
- Liu, M.; Zhang, K.; Liang, Y.; Yang, Y.; Chen, Z.; Liu, W. Life Cycle Environmental and Economic Assessment of Electric Bicycles with Different Batteries in China. *J. Clean. Prod.* **2023**, *385*, 135715. [[CrossRef](#)]
- Allen, C.; Telford, C. *Automotive Battery Technology Trends Review*; Ricardo Strategic Consulting (RSC): Shoreham-by-Sea, UK, 2020.
- Sagastume, A.; Cabello, J.J.; Huisingh, D.; Vandecasteele, C.; Hens, L. The Current Potential of Low-Carbon Economy and Biomass-Based Electricity in Cuba. The Case of Sugarcane, Energy Cane and Marabu (*Dichrostachys Cinerea*) as Biomass Sources. *J. Clean. Prod.* **2018**, *172*, 2108–2122. [[CrossRef](#)]
- Yu, Y.; Mao, J.; Li, C. Historical Evolution of Lead-Acid Battery System and Its Relationship with External Environment Based on the Composite Flow. *Sci. Total Environ.* **2020**, *707*, 134746. [[CrossRef](#)]
- Sullivan, J.L.; Gaines, L. *A Review of Battery Life-Cycle Analysis: State of Knowledge and Critical Needs*; Energy Systems Division: Chicago, IL, USA, 2010.
- Sullivan, J.L.; Gaines, L. Status of Life Cycle Inventories for Batteries. *Energy Convers Manag.* **2012**, *58*, 134–148. [[CrossRef](#)]
- Rydh, C.J.; Sandén, B.A. Energy Analysis of Batteries in Photovoltaic Systems. Part I: Performance and Energy Requirements. *Energy Convers Manag.* **2005**, *46*, 1957–1979. [[CrossRef](#)]
- Rantik, M. *Life Cycle Assessment of Five Batteries for Electric Vehicles under Different Charging Regimes*; Master, Swedish Transport and Communications Research Board: Stockholm, Sweden, 1999.
- Davidson, A.J.; Binks, S.P.; Gediga, J. Lead Industry Life Cycle Studies: Environmental Impact and Life Cycle Assessment of Lead Battery and Architectural Sheet Production. *Int. J. Life Cycle Assess.* **2016**, *21*, 1624–1636. [[CrossRef](#)]
- Yudhistira, R.; Khatiwada, D.; Sanchez, F. A Comparative Life Cycle Assessment of Lithium-Ion and Lead-Acid Batteries for Grid Energy Storage. *J. Clean. Prod.* **2022**, *358*, 131999. [[CrossRef](#)]
- Balbis, M.; Cabello, J.J.; Sagastume, A.; Sousa, V.; Pérez, Y.; Rueda-Bayona, J.G. Factors Affecting the Electricity Consumption and Productivity of the Lead Acid Battery Formation Process. The Case of a Battery Plant in Colombia. *Int. J. Energy Econ. Policy* **2019**, *9*, 103–112. [[CrossRef](#)]
- ElMaraghy, H.A.; Youssef, A.M.A.; Marzouk, A.M.; ElMaraghy, W.H. Energy Use Analysis and Local Benchmarking of Manufacturing Lines. *J. Clean. Prod.* **2017**, *163*, 36–48. [[CrossRef](#)]
- Sa, A.; Thollander, P.; Cagno, E. Assessing the Driving Factors for Energy Management Program Adoption. *Renew. Sustain. Energy Rev.* **2017**, *74*, 538–547. [[CrossRef](#)]
- Paramonova, S.; Thollander, P.; Ottosson, M. Quantifying the Extended Energy Efficiency Gap—Evidence from Swedish Electricity-Intensive Industries. *Renew. Sustain. Energy Rev.* **2015**, *51*, 472–483. [[CrossRef](#)]

20. Cagno, E.; Trianni, A. Evaluating the Barriers to Specific Industrial Energy Efficiency Measures: An Exploratory Study in Small and Medium-Sized Enterprises. *J. Clean. Prod.* **2014**, *82*, 70–83. [[CrossRef](#)]
21. Jovanović, B.; Filipović, J.; Bakić, V. Energy Management System Implementation in Serbian Manufacturing—Plan-Do-Check-Act Cycle Approach. *J. Clean. Prod.* **2017**, *162*, 1144–1156. [[CrossRef](#)]
22. Brunke, J.C.; Johansson, M.; Thollander, P. Empirical Investigation of Barriers and Drivers to the Adoption of Energy Conservation Measures, Energy Management Practices and Energy Services in the Swedish Iron and Steel Industry. *J. Clean. Prod.* **2014**, *84*, 509–525. [[CrossRef](#)]
23. Fernando, Y.; Hor, W.L. Impacts of Energy Management Practices on Energy Efficiency and Carbon Emissions Reduction: A Survey of Malaysian Manufacturing Firms. *Resour. Conserv. Recycl.* **2017**, *126*, 62–73. [[CrossRef](#)]
24. Carpenter, J.; Woodbury, K.A.; O'Neill, Z. Using Change-Point and Gaussian Process Models to Create Baseline Energy Models in Industrial Facilities: A Comparison. *Appl. Energy* **2018**, *213*, 415–425. [[CrossRef](#)]
25. Kiessling, R. Lead Acid Battery Formation Techniques. *Digatron Firing Circuits Digatron* **1992**, 1–31.
26. Zanconato, M.D.; de Rossi, B.B.; Johansen, H.D.; Chaves, M.R.d.M.; Antoniassi, B. Automation Benefits in the Formation Process of Lead-Acid Batteries. *Indep. J. Manag. Prod.* **2017**, *8*, 91–107. [[CrossRef](#)]
27. Cabello, J.J.; Sagastume, A.; Sousa, V.; Cabello, M.J. Energy Management of Compressed Air Systems. Assessing the Production and Use of Compressed Air in Industry. *Energy* **2020**, *213*, 118662. [[CrossRef](#)]
28. *ISO 50001:2018*; Energy Management Systems—Requirements with Guidance for Use. ISO: Geneva, Switzerland, 2018.
29. *ISO 50006*; Energy Management Systems—Measuring Energy Performance Using Energy Baselines (EnB) and Energy Performance Indicators (EnPI)—General Principles and Guidance. ISO: Geneva, Switzerland, 2014.
30. Wegener, M.; Isalgue, A.; Malmquist, A.; Martin, A.; Santarelli, M.; Arranz, P.; Camarra, O. Exergetic Model of a Small-Scale, Biomass-Based CCHP/HP System for Historic Building Structures. *Energy Convers. Manag. X* **2021**, *12*, 100148. [[CrossRef](#)]
31. Bohdanowicz, P.; Martinac, I. Determinants and Benchmarking of Resource Consumption in Hotels—Case Study of Hilton International and Scandic in Europe. *Energy Build.* **2007**, *39*, 82–95. [[CrossRef](#)]
32. Puranik, V.S. CUSUM Quality Control Chart for Monitoring Energy Use Performance, 2007. In Proceedings of the IEEM 2007: 2007 IEEE International Conference on Industrial Engineering and Engineering Management, Singapore, 2–5 December 2007; IEEE: Singapore, 2007; pp. 1231–1235.
33. Lin, B.; Recke, B.; Knudsen, J.K.H.; Jørgensen, S.B. A Systematic Approach for Soft Sensor Development. *Comput. Chem. Eng.* **2007**, *31*, 419–425. [[CrossRef](#)]
34. Katronic Katronic Download Centre. Available online: <https://www.katronic.com/pages/katronic-datasheets-manuals-and-application-references-for-downloading/> (accessed on 26 April 2023).
35. Teledyne FLIR Support for FLIR E53. Available online: <https://www.flir.com.mx/support/products/e53/#Documents> (accessed on 26 April 2023).
36. TESTO Testo 340—Flue Gas Analyzer for Industry. Available online: <https://www.testo.com/en-ID/testo-340/p/0632-3340> (accessed on 28 June 2022).
37. Stevenson, M. Encyclopedia of Electrochemical Power Sources. In *Encyclopedia of Electrochemical Power Sources*; Garcke, J., Ed.; Elsevier: Amsterdam, The Netherlands, 2009; pp. 165–178. ISBN 9780444527455.
38. Kermeli, K.; Deuchler, R.; Worrell, E.; Masanet, E. *Energy Efficiency and Cost Saving Opportunities for Metal Casting an ENERGY STAR® Guide for Energy and Plant Managers*; US EPA: Washington, DC, USA, 2016.
39. Minnesota Technical Assistance Program Energy Efficiency Opportunities for Ferrous Metal Casters. Available online: <http://www.mntap.umn.edu/industries/facility/metalcast/ferrous/> (accessed on 28 June 2022).
40. ITP Metal Casting. *Advanced Melting Technologies: Energy Saving Concepts and Opportunities for the Metal Casting Industry*; U.S. Department of Energy: Columbia, IN, USA, 2005.
41. Azeez, R.O.; Bashiru, A.; Olufemi, O.; Olakunle, O.T.; Oludele, A. Development of a High-Efficiency Crucible Furnace for Melting 30kg Non-Ferrous Metal Scraps. *Am. J. Eng. Res.* **2020**, *9*, 62–70.
42. Kirchner, R.L. *Electric Resistance Melting: A Low Cost, Efficient Method for the Melting and Heating of Aluminum and Other Metals*; The EPRI Center for Metals Product: Pennsylvania, PA, USA, 1986.
43. UNIDO. *Independent Mid-Term Evaluation. Promoting Energy Efficiency and Renewable Energy in Selected Micro, Small and Medium Enterprises (MSME) Clusters in India*; UNIDO: Vienna, Austria, 2018.
44. Szakacs, B.; Scratish, F. Lead Acid Battery Grid Casting System Installation and Technique. U.S. Patent 4,090,550, 23 May 1978.
45. Knospe, B. *Practical Guide Industrial Flue Gas Analysis*; Testo: Alton Hampshire, UK, 2018.
46. U.S. Department of Energy. *Improving Process Heating System Performance: A Sourcebook for Industry*, 2nd ed.; Industrial Technologies Program: Washington, DC, USA, 2007; pp. 1–116.
47. U.S. Department of Energy. *Improving Process Heating System Performance: A Sourcebook for Industry*, 3rd ed.; U.S. Department of Energy: Washington, DC, USA, 2015.
48. Hebei United Energy Tech Non-Combustible Mineral Wool Insulation. Available online: [https://www.alibaba.com/product-detail/Mineral-Wool-Thermal-Conductivity-Price-Mineral\\_1600121804484.html?spm=a2700.7724857.normal\\_offer.d\\_title.32b058b3MMhNVL&s=p](https://www.alibaba.com/product-detail/Mineral-Wool-Thermal-Conductivity-Price-Mineral_1600121804484.html?spm=a2700.7724857.normal_offer.d_title.32b058b3MMhNVL&s=p) (accessed on 28 October 2021).
49. Bejan, A. *Convection Heat Transfer*, 4th ed.; John Wiley & Sons: Hoboken, NJ, USA, 2013; ISBN 9780470900376.

50. Bergman, T.L.; Lavine, A.S.; Incropera, F.P.; DeWitt, D.P. *Fundamentals of Heat and Mass Transfer*, 7th ed.; John Wiley & Sons: Hoboken, NJ, USA, 2011.
51. Churchill, S.W.; Chu, H.H.S. Correlating Equations for Laminar and Turbulent Free Convection from a Vertical Plate. *Int. J. Heat. Mass. Transf.* **1975**, *18*, 1323–1329. [[CrossRef](#)]
52. Boetcher, S.K.S. *Natural Convection from Circular Cylinders*; Springer: New York, NY, USA, 2014; ISBN 9783319081311.
53. Martynenko, O.G.; Khramtsov, P.P. *Free-Convective Heat Transfer*; Springer: Berlin/Heidelberg, Germany, 2005; ISBN 9783540250012.
54. Kang, G.U.; Chung, B.J.; Kim, H.J. Natural Convection Heat Transfer on a Vertical Cylinder Submerged in Fluids Having High Prandtl Number. *Int. J. Heat. Mass. Transf.* **2014**, *79*, 4–11. [[CrossRef](#)]
55. Valero, A.; Valero, A. Chemical Exergy Calculator. Available online: <https://www.exergoecology.com/excalc> (accessed on 8 March 2022).
56. UPME Calculadora de Emisiones. Available online: [http://www.upme.gov.co/calculadora\\_emisiones/aplicacion/calculadora.html](http://www.upme.gov.co/calculadora_emisiones/aplicacion/calculadora.html) (accessed on 18 May 2023).
57. CML—Department of Industrial Ecology. *CML-IA Characterisation Factors*; CML—Department of Industrial Ecology: Leiden, The Netherlands, 2016.
58. Kusik, C.L.; Kenahan, C.B. *Energy Use Patterns for Metal Recycling*; U.S. Government Printing Office: Washington, DC, USA, 1978.
59. Prabhakar, A.; Mielnicka, J.; Jolly, M.; Salonitis, K. Improving Energy Efficiency in Direct Method for Continuous Casting of Lead Sheets. In *The Minerals, Metals & Materials Series*; Springer: Cham, Switzerland, 2018; Pt F6, pp. 121–132. [[CrossRef](#)]
60. Bouras, F.; Attia, M.E.H.; Khaldi, F. Entropy Generation Optimization in Internal Combustion Engine. *Environ. Process.* **2015**, *2*, S233–S242. [[CrossRef](#)]
61. Çengel, Y.A.; Ghajar, A.J. *Heat and Mass Transfer: Fundamentals and Applications*, 6th ed.; McGraw-Hill Education: New York, NY, USA, 2019; ISBN 978-0073398198.
62. Frogner, K.; Andersson, M.; Cedell, T.; Svensson, L.; Jeppsson, P.; Ståhl, J.-E. Industrial Heating Using Energy Efficient Induction Technology. In Proceedings of the Proceedings of the 44th CIRP International Conference on Manufacturing Systems, Madison, WI, USA, 31 May–3 June 2011.
63. Chromalox Impedance Heating System. Available online: <https://www-dev.chromalox.com/catalog/industrial-heaters-and-systems/heat-transfer-system/impedance-heating-systems/impedance-heating-system> (accessed on 6 December 2021).
64. Sandia National Laboratories. *Heat Trace Options Report*; Sandia National Laboratories: Albuquerque, NM, USA, 2019.
65. Sandia National Laboratories. *Preheating System Comparison*; Sandia National Laboratories: Albuquerque, NM, USA, 2019.

**Disclaimer/Publisher’s Note:** The statements, opinions and data contained in all publications are solely those of the individual author(s) and contributor(s) and not of MDPI and/or the editor(s). MDPI and/or the editor(s) disclaim responsibility for any injury to people or property resulting from any ideas, methods, instructions or products referred to in the content.